Non-Coherent Radio-Based Positioning

MOHAMAD ABOU NASA
FARSHID REZAEI
MASTER´S THESIS
DEPARTMENT OF ELECTRICAL AND INFORMATION TECHNOLOGY
FACULTY OF ENGINEERING | LTH | LUND UNIVERSITY

Non-Coherent Radio-Based Positioning

Mohamad Abou Nasa
mo8536ab-s@student.lth.se

Farshid Rezaei
fa8257re-s@student.lu.se

Department of Electrical and Information Technology
Lund University

Supervisor: Fredrik Tufvesson and Xuhong Li

Examiner: Fredrik Rusek

August 29, 2019

Printed in Sweden
Tryckeriet i E-huset, Lund

Abstract

In this thesis, a new Angle-of-Arrival (AoA) technique is used to determine the direction of a target in an outdoor environment using Radio Frequency (RF) signals. This technique estimates the AoA based on the difference between the Received Signal Strength Indicators (RSSI) from two/four directive antennas. This thesis work includes a mathematical model for this new technique, simulations that matches real life scenarios, and many measurements in real environments. The main task is a proof-of-concept for the RSSI difference-based AoA. In order to test the developed algorithm two communication technologies were used, Bluetooth Low Energy (BLE), and Long Range Wide Area Network (LoRaWAN). Both technologies are power efficient systems and are widely used in Internet of Things (IoT); BLE is used for short range applications while LoRa is used for long range applications. Two estimation techniques were developed based on hard decisions, but the core for both estimation techniques was the same. The difference was in the number of antennas used in each setup and the estimation procedure. The obtained results complied with the theoretical expectations. Though there was some range issues in the LoRa case. The results looked promising and the next step for this thesis work is to use more advanced estimation techniques in order to enhance the accuracy of AoA, and to work on suggested solutions for the LoRa issues.

Acknowledgments

First and foremost, we would like to thank our advisors, Professor Fredrik Tufvesson, for giving us the chance to work with him and for his advice, comments, discussions, and feedback throughout the whole thesis, and our second advisor Xuhong Li, for her help, support, and all the fruitful discussions for duration of this thesis. The outcome of this thesis would not have been possible without their supervision and guidance. We would, also, like to thank the EIT department at Lund University for giving us the opportunity to complete our studies in an exciting research environment. Finally, we would like to thank our families and friends for their emotional support, encouragements, and patience.

Popular Science Summary

Advances made in technology have paved the way for many new technologies. One of such advances are those made in the field of Internet of Things (IoT). These advances have received much attention in academia, industry, as well as in society. Advances that made it possible to manufacture miniature electronics chips that are power efficient made it possible to provide solutions to many difficult situations. In addition, they can be used in planning smart cities and vehicles.

In most of big cities, and nowadays, smaller cities, many services that were not available a few years ago can be found; some of such services are bicycles and scooters that can be rented by anyone by simply downloading the services' applications and use them to find a nearby bicycle or scooter. Another situation where these technologies become handy are the cases of lost animals, key-chains, or any other object.

These new advances made it possible to manufacture small chips/devices that are implantable, wearable, or can be attached to any desired object. As an example, a small chip can be attached to an animal's collar and use an applicable application to locate the animal. Or in the case of key-chains or other objects, attach the chip to the desired object to make it easier to find.

One of such technologies is Bluetooth Low Energy or simply BLE. Depending on how frequent a device equipped with BLE is used, it can work for weeks, months, or even a year without any need to replace its battery. Such devices are very useful when a permanent source of energy is not usually available or changing the batteries on a frequent bases is not applicable.

One of the fields in which these devices are useful is the field of animal tracking where scientists implant or put a tag on an animal or a group of animals and study their behavior. This is very helpful in finding the where-about of animals and can be used to prevent poaching and illegal hunting. In this thesis, a new technique that can be used implementing both BLE or LoRa technologies was developed for positioning. Additionally, the new technique is considered to be simpler than most of the technologies currently in use.

Table of Contents

List of Figures

List of Tables

Acronyms

3G 3rd Geneartion Cellular Network Technology

4G 4th Geneartion Cellular Network Technology

5G 5th Geneartion Cellular Network Technology

AP Access points

AoA Angle-of-Arrival

BLE Bluetooth Low Energy

BR Basic Rate

c2c center-to-center distance between the two antennas

CSS Chirp Spread Spectrum

DPSK Differential Phase-Shift Keying

DQPSK Differential Quadrature Phase-Shift Keying

EDR Enhanced Data Rate

FHSS Frequency-Hopping Spread Spectrum

FSK Frequency Shift Keying

GFSK Gaussian Frequency Shift Keying

GPS Global Positioning System

IEEE Institute of Electrical and Electronics Engineers

IoT Internet of Things

ISM Industrial, Scientific, and Medical

LLS Linear Least Square

LoRa Long Range

LoRaWAN Long Range Wide Area Network

LoS Line of Sight

LPWAN Low-Power Wide-Area Network

LS Least Square

LSF Large-Scale Fading

MC Monte-Carlo

MIMO Multiple Input Multiple Output

NLoS Non-Line of Sight

PDF Probability Density Function

PL Path-Loss

PLE Path Loss Exponent

RMSE Root-Mean-Square Error

RF Radio Frequency

RSS Received Signal Strength

RSSI Received Signal Strength Indicator

ΔRSSI RSSI Difference

RX Receiver

SSF Small-Scale Fading

std standard deviation

TA Target

TDoA Time Difference of Arrival

ToA Time of Arrival

TTN The Things Network

TX Transmitter

WLLS Weighted Linear Least Square

WPAN Wireless Personal Area Network

Chapter 1

Introduction

The development in the wireless communication field has taken a huge step toward an expansion of the applications that are driven by the radio signals. 5th Geneartion Cellular Network Technology (5G) and Internet of Things (IoT) hot topics in the field of wireless communications nowadays [1]; millions of nodes and sensors are expected to be deployed in the coming years [2]. The development calls for new localization systems that are power efficient and low cost unlike the Global Positioning System (GPS) that is the most known localization system for outdoor environments [3]. The choice of a final solution for the outdoor environments that complies with the requirements of IoT is still under development.
Localization techniques, typically, use the received signal's time, power and phase in order to determine the location of the Target (TA) [4]. However, reputation of localization techniques that are based on Received Signal Strength (RSS) is so low due to the sensitivity of power to the channel/propagation conditions that leads to low accuracy in position estimation [5]. For that, most of the localization systems that use RSS, combine it with time and/or Angle-of-Arrival (AoA), in order to achieve higher accuracy for the estimated position.
AoA based on Received Signal Strength Indicator (RSSI) difference was mentioned in [7], where two perpendicular directive antennas were used for estimating the angle of arrival from 0° to 90°; there, it was used for indoor environments. For this thesis work, the AoA based on RSSI Difference (ΔRSSI) is used to estimate AoA for a wider range of angles i.e. from 0° to 180° in an outdoor environment. It should be mentioned that with the use of more antennas it can estimate the AoA for the full angular range. This chapter provides a brief study about the background of the theory behind the proposed technique. At the end of this chapter, there is the problem formulation section were the aims, motivations, and expectations for this project are defined. Chapter 2 explains the proposed AoA estimation technique. Chapter 3 gives an overview for the algorithms used for positioning. Chapter 4 is the chapter where the proposed AoA estimator testing environment is defined, and it includes results of real time measurements in regard with the accuracy of the estimated AoA and position estimates. In Chapter 5, the AoA sector estimator and a four-antenna setup using Long Range (LoRa) technology is used; this chapter includes different test environments. Conclusions and future work are given in the last two chapters.

1.1 AoA Estimation

AoA is one of the standard techniques used for position estimation, where the TA broadcasts a signal toward a Receiver (RX) equipped with an array of antennas. The time information from each element in this array are most commonly used techniques for the estimation of the AoA [4]. In this thesis work, the RSS is considered instead. So that the elements in the array will receive different powers based on the shape of the radiation pattern and its characteristics. ΔRSSI-based AoA estimation is not widely used, which drives the challenge for the authors to come with a technique that can achieve accurate estimate of AoA which is more accurate than that of the phase difference techniques. More details about the proposed technique can be found in the next chapter.

1.2 Position Estimation

Position estimation techniques usually relies on the information collected from three or more Access points (AP)s in order to determine the position of the TA. Most common techniques depend on measured RSSI value, AoA, Time Difference of Arrival (TDoA), or combinations of two or more of these [6]. In this section, positioning based on RSSI, AoA and a hybrid RSSI/AoA are explained.

1.2.1 Trilateration

Trilateration is a method to determine the location of a moving/stationary TA in space using multiple ranges (distances) between the TA and three or more spatially-separated AP with known locations [8][9]. In a noise free environment, each AP will estimate a range based on the measured RSSI value. These estimated ranges, as depicted in Figure 1.1b, are then used to draw a circles around each AP with radii equal to those range estimates. In such scenarios, when noise is absent, all the circles intersect at a point which is the TA's position. In the presence of noise, the measured RSSI values will give inaccurate range estimates. This will, in turn, prevent those circles from intersecting at one point but instead define an area bordered by those circles as shown in Figure 1.1a in which the TA is likely to lie within. The stronger the present noise the wider the defined area becomes and the more inaccurate the position estimate. Nevertheless, this technique can still be used in various application where highly accurate position estimation is not required.

1.2.2 Triangulation

Triangulation is a method to determmine the location of the TA using the information available about the direction of TA i.e. AoA is used to draw a line from the AP to the TA. Here, by using at least two APs, the TA's location is determined by using trigonometry laws of sine and cosine [10]. Triangulation is the technique of determining the location of a target by forming triangles to the TA from two or more access points as in Figure 1.2. Again, noise affects the position estimation

with Triangulation. In such cases, at least three APs are needed to estimate a region that should contain the target position [4].

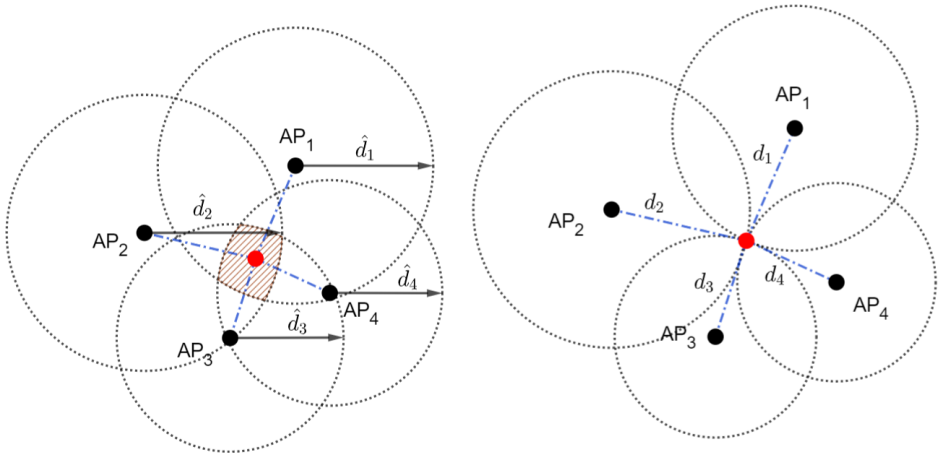

(a) Trilateration in the presence of noise. **(b)** Noise free trilateration.

Figure 1.1: Trilateration.

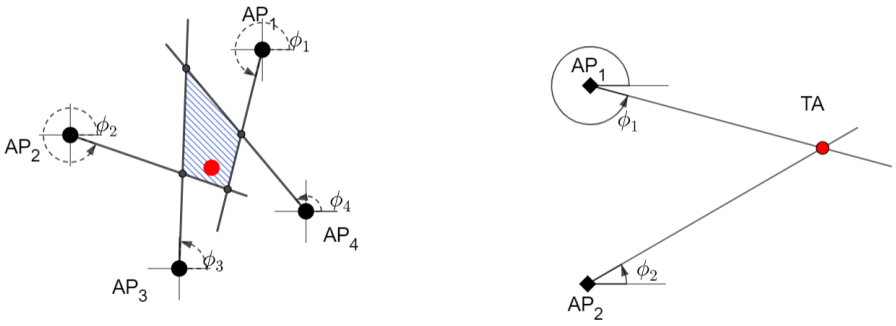

(a) Triangulation in the presence of noise. **(b)** Noise free triangulation.

Figure 1.2: Triangulation.

1.2.3 Hybrid RSSI/AoA Model

Hybrid systems can estimate the position of a target using combined positioning techniques. In this section a hybrid model is considered, so that range and AoA are combined to give one position estimate from three or more access points. Figure 1.3 is the result of when the case in Figure 1.1a and Figure 1.2a are combined. It can be seen that the region in which the TA is located becomes smaller when the two techniques are combined. This will result in less inaccuracy in position

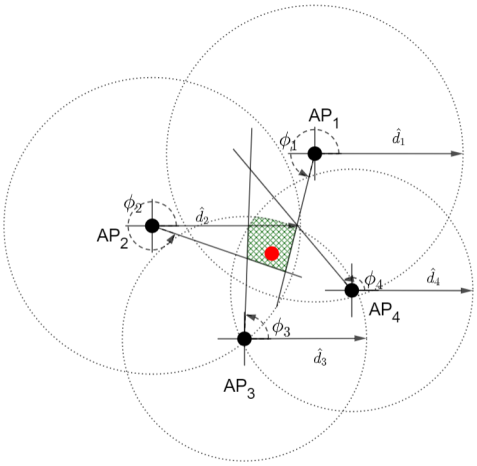

Figure 1.3: Hybrid RSSI/AoA Model.

estimation [6]. As it can be seen in the Figure 1.3, that the region of uncertainty is minimized, since the position estimation is dependent on two factors instead of one factor. For that, the authors used this model during the thesis work. The position estimation techniques based on the hybrid model is explained in Chapter 4.

1.3 Purpose and Aims

The aim of this project is to develop a new positioning technique, that is highly accurate, suitable for outdoor long/short range scenarios, can be used for online and offline processing, compatible with power efficient systems, and works well in Line of Sight (LoS) and Non-Line of Sight (NLoS) environments. The new positioning technique will estimate the TA position using the AoA and range estimates. Both AoA and range are estimated using the RSSI values. *We would like to emphasize that our positioning algortihm does not use any phase information, but relies solely on amplitude information.* The main task of this project is to make an estimate that is highly accurate and is immune to channel/propagation conditions from RSSI values that are sensitive to these conditions. The objectives for this project are to achieve AoA accuracy of 10° in LoS scenarios and 20° in the NLoS scenarios, to achieve position accuracy in LoS scenario for the short range communication system of 1 m and 10 m for the long range communication system, and to have position accuracy for the long range communication system in a NLoS scenario of 100m. In this thesis work answer to following questions are provided:

- What is the theory behind the new AoA estimation technique?
- Is it achieving highly accurate AoA estimates from a noisy fragile parameter RSSI? and why?
- What are the assumptions and the limitation of the proposed technique?

- What are the factors that affect/determine the AoA estimation?
- Are the objective and aims are achieved? and why?

1.4 Methodology

In order to achieve the set of objectives that were defined in the previous section and to answer the research questions, the following methodology is followed. Firstly, the relation between the AoA and RSSI difference is studied so that a closed form relation is expected to be derived. Then the physical theory of the this mathematical model is studied in order to check the validity of the concept. After that, the conditions that determines the validity of the derived model is studied in order to answer the question of what/when the derived model is valid. An estimator that can achieve the desired accuracy should be developed and after that the measurements can take place. Three different types of measurements are planned to be conducted: the channel/propagation statistics measurement that will check the validity of the conditions/assumptions for the proposed technique. The second measurements set is to check the accuracy of the AoA in LoS and NLoS scenarios. The third measurement is to evaluate the AoA estimation technique in a positioning system and estimate the position based on the AoA estimates. All details about measurement setups, hardware, and communication technologies used will be explained extensively through the text. At the end, the final conclusions and results will be presented.

Chapter 2

AoA Estimation

2.1 Introduction

ΔRSSI-based AoA estimation is an approach that depends on the radiation pattern of the antennas [7]. The difference between the RSSI values can be simplified into a gain difference; and this gain difference is used to determine the angle of arrival from a reference point C that lies on the intersection of the perpendicular lines from the centers of the two antennas, see Figure 2.1. Using this estimated AoA at point C and using the physical geometry of the used antenna setup, AoA at each receiving antenna can be obtained.

The proposed algorithm can estimate the AoA using just two antennas at the AP, but increasing the number of antennas at the AP will result in more combinations between the RSSI values received by the antennas at one AP, so instead of having one AoA estimate from one RSSI difference, AoA can be estimated from more than one RSSI differences; which improves the AoA estimation accuracy. In this thesis, two different antenna setups were used, the first one is a dual-antenna setup operating in the 2.4 GHz frequency band, and the second one is a four-antenna setup operating in the 868 MHz frequency band. Both of the approaches will estimate the AoA using a lookup table, that is generated according to specific parameters, and these parameters will influence the performance of the AoA estimation.

In this thesis work, identical directive radiation patterns were considered; it is critical for this approach to choose the best suitable separation angle between the antennas.

For the AoA estimator to give the best possible results there are many assumptions that should apply, such as Small-Scale Fading (SSF) mitigation, and that both antennas are experiencing the same propagation conditions, and some other factors that will be explained later in this chapter.

2.2 Derived Relation Between RSSI Difference and AoA

Starting from the definition of RSSI which is obtained using Friis transmission equation for the received power as in Equation (2.1) [18]. It can be seen that the received power depends on many parameters that effect its value. Parameters such as the transmitted power and gains of both transmitting/receiving antennas

increase the value of RSSI while parameters such as Path-Loss (PL), Large-Scale Fading (LSF) and Small-Scale Fading (SSF) will decrease the value of the RSSI,

$$P_{RX} = P_{TX} + G_{TX} + G_{RX} - 10\eta \log d + SSF + LSF, \tag{2.1}$$

where, P_{RX} is the received power, P_{TX} is the transmitted power, G_{TX} and G_{RX} are transmitter and receiver gain respectively, η is the path-loss exponent and SSF and LSF are small scale fading and large scale fading respectively. Note that all the quantities here are in dB scale. Taking the difference between the RSSI values at the same time instance results in removal of common parameters such as P_{TX} and G_{TX}. This gives ΔRSSI equation as:

$$\Delta RSSI = G_{RX_1} - G_{RX_2} - 10\eta_1 \log d_1 + 10\eta_2 \log d_2 + SSF_1 - SSF_2 + LSF_1 - LSF_2, \tag{2.2}$$

LSF_1 and LSF_2 can be considered to be highly correlated since the distance of separation between the antennas is relatively small with respect to the range between the TA and the AP. Hence, it can be assumed that both antennas suffer from the same shadowing effect. As for the SSF, it is assumed that averaging large number of samples within a relatively short time duration mitigates their effect and can be neglected. It should be mentioned here that averaging is dependent on the used communication technology. Therefore, how frequent is the transmission and how good is the reception determines if averaging can be used. For example, in LoRa case it is hard to receive high number of samples within a short time interval due to low frequency of transmission. On the hand, for Bluetooth Low Energy (BLE) the number of samples within the same short interval is so high. Next, what remains is the distant dependant term, PL. From Equation (2.2), it can be seen that only a small part of the distance dependency remains; this part is the small difference between ranges seen by each antenna at the AP. Since this difference is considerably small compared to the range from the TA, it is considered negligible. As it was mentioned before, the propagation conditions are assumed to be the same on both antennas and so, η_1 and η_2 will be considered to be the same. As a result, a direct relation between ΔRSSI and the gains of the two RXs is obtained as shown in Equation (2.3):

$$\Delta RSSI = G_{RX1}(\phi_1) - G_{RX2}(\phi_2), \tag{2.3}$$

where ϕ is the AoA of the signal in the azimuth plan at the center point C between the antennas. Thus, the relation between AoA and ΔRSSI is an inverse function where having one term measured will directly give the other term's value. And this direct relation is the proposed AoA estimation algorithm that will be discussed extensively later in this chapter. For best result, It is important to have antennas with identical radiation patterns at the AP.

In case that these assumptions do not apply, the noise term ζ is added to Equation (2.2), ζ is from the small difference between the Path Loss Exponent (PLE), or from the remaining SSF part after averaging, or if the LSF is not fully correlated at the receiving antennas.

$$\Delta RSSI = G_{Rx1}(\phi_1) - G_{Rx2}(\phi_2) + \zeta, \tag{2.4}$$

As a result of this noise the AoA estimates will experience a deviation from its ground truth value that will lead to a wrong estimation, the value of this noise term and its effect will be investigated later in this chapter.

2.3 Proposed AoA Algorithm/Estimator and Setups

As ΔRSSI and AoA are directly related, an AoA table will be built according to the difference between the antenna gains; the gains are ground truth values from the radiation patterns which are either measured or generated synthetically, a table of AoA is formed from 0°-180° in order to cover the area facing the antennas in the azimuth plane as it can be seen in Figure 2.1, where G_1 and G_2 are the receiver gains of antenna 1 and antenna 2 respectively, ϕ_c is the estimated AoA resulting from ΔRSSI, and the target movement is in the region from 0° to 180°.

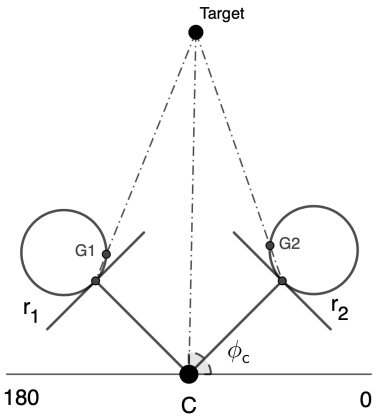

Figure 2.1: Geometrical setup of the receive antennas and a target node.

The resulting table will contain ΔRSSI values and the corresponding angle of arrivals, Figure 2.2 shows the plot of ΔRSSI values against angle of arrivals. As it can be seen, this curve can be divided into three regions, where the first region is from 0° to 60° where each ΔRSSI value corresponds to two AoAs and the ΔRSSI values are negative, the second region is where AoA lies between angles 60° and 120°; in this region, ΔRSSI values corresponds to just one AoA. While in the third region, AoA is between 120° and 180° where ΔRSSI values are positive and correspond to two AoAs. The first and the third regions will be referred to as "ambiguity" regions and the second region will be referred to as "linear" region in the rest of the text. The proposed algorithm will estimate the AoAs based on this look-up table that is generated using the synthetic radiation pattern of the receiving antennas. This pattern is shown in Figure 2.3, where the 3 dB beam-width and the separation angle between the antennas will determine the region from the minimum to the maximum of the look-up table, while the side lobes in the radiation pattern and the separation angle will determine the regions from 0°

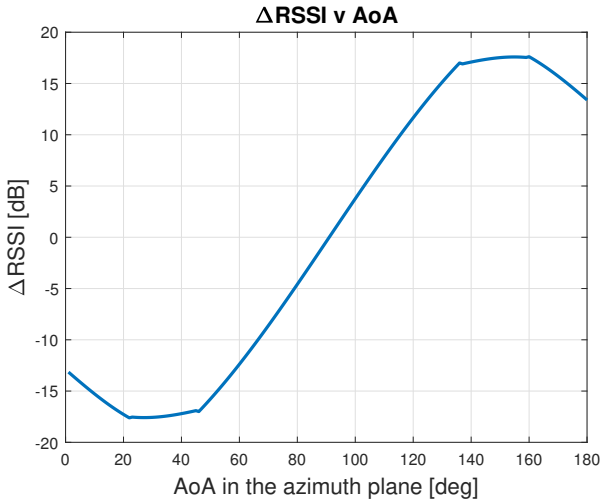

Figure 2.2: ΔRSSI versus AoA at sep.angle 90° and sep.distance 1λ.

to 21° and from 159° to 180°.

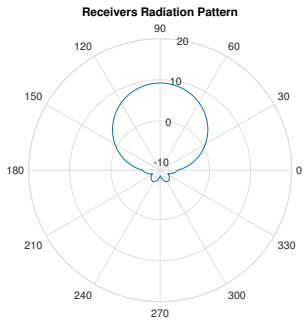

Figure 2.3: Receiving Antenna Synthetic Radiation Pattern.

The look-up table is determined by the selected separation angle; i.e. the linear region will increase as the separation angle increases, which is desired. However, when the separation angle is increased, the ambiguity region becomes flatter and, hence, it becomes difficult to distinguish between angles in that region. An effect that is not desired and wanted to be avoided. To explain, having a flat ambiguity region means that for 1 dB or 2 dB ΔRSSI, there will be 30 to 40 values for AoA that correspond ΔRSSI values.

Obviously, the width and flatness of the ambiguity region and linearity of the linear region are dependent on the separation angle between the antennas. Figure 2.4 shows how the S-shaped ΔRSSI against AoA varies for different separation angles between the antennas and for 3 dB beam-width that is equal to 60° azimuth. In this figure, it is noticed that the smaller is the separation angle the smaller is

the difference between the minimum and the maximum value of the ΔRSSI which implies that the angular resolution becomes smaller with smaller angle separation and vice versa. To decide which separation angle should be the best is dependent on the application, and the physical size of the antennas, since directive antennas sizes are proportional to the signal's wavelength. In order to have larger angular resolution between consecutive AoAs, a larger angle separation must be selected. The trade off here, however, is the size of the ambiguity region. It should be noted also that noisy ΔRSSI will cause the AoA to deviate from its ground truth value; so, having a steeper linear region on the S-shape means that there are larger differences between consecutive ΔRSSI and hence, it is easier to distinguish between AoAs corresponding to the values of the ΔRSSI. This, in turn, lowers the error in AoA estimates and increases the angular accuracy of the estimator. One can note that this look-up table essentially is the same as performing linear regression in the non-ambiguous region of the S-shape.

The next sections will explain more about AoA estimation based on these look-up tables.

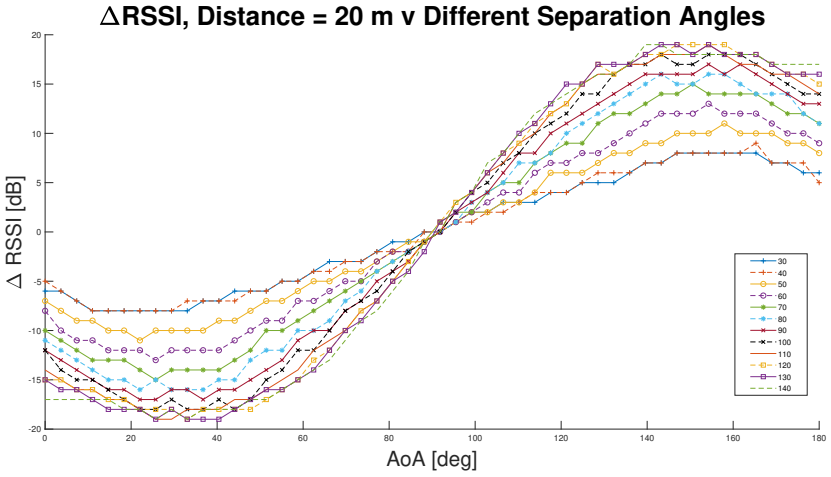

Figure 2.4: $\Delta RSSI$ v AoA for different separation angles.

In addition to the separation angle that influences the look-up table, another factor should be studied as well. This is the c2c, see Figure 2.5. Figure 2.5 shows that the c2c is irrelevant and its effect can be discarded. It can be concluded that what matters for the gain difference is the amplitude of the received signals not the phase, since c2c is so small compared to the range. After studying the effect of the separation angle and the separation distance between the antennas, the shape of the radiation pattern of the receiving antennas, the look-up table is generated according to these values. In the next sections, will describe the procedure of using this look-up tables in different antenna setups.

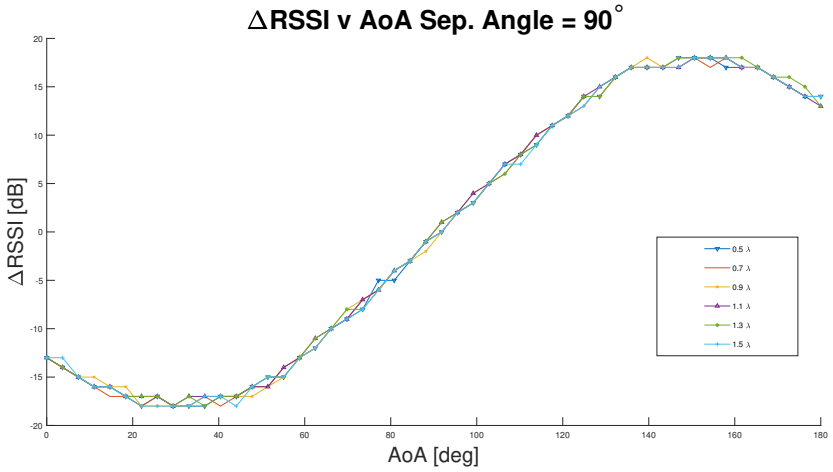

Figure 2.5: $\Delta RSSI$ versus AoA for different c2c separations.

2.3.1 Dual-Antenna Setup

In this section two antennas at one AP is considered, so that only one look-up table will be generated according to the separation angle between the antennas and it will be used in order to estimate the AoA; the dual-antenna setup is shown in Figure 2.1. As it can be seen in Figure 2.4, the best possible AoA for the dual-antenna setup is the 90° separation angle. That is because the linear region is from 60° to 120°, and the ambiguity regions are from 0° to 60° and 120° to 180°. In order to find a solution to differentiate between the estimated angles in the ambiguity region, RSSI sum in linear and dB domain was studied but there was no proper solution since they are distance dependent and so it was not possible to find a closed form solution that could differentiate between these angles. So without considering any time/phase information from the received signal and depending only on the amplitude of the received signals it was not applicable to use the RSSI sum. As a result, the look-up table for dual-antenna setup will be taken from minimum to the maximum of the ΔRSSI against the AoA curve. In order to have just one AoA estimate for each ΔRSSI value, the look-up table was limited to be from 30° to 150°. So for the a target in the region from 0° to 30° the estimated angles would be 60° to 30°. This means that each AoA estimate in the ambiguity region will have different variance value, that will limit the performance of the AoA estimator. The same holds for the AoA estimates in the 150° to 180° region. Note that the relation between ΔRSSI and AoA follows a S-shaped curve. The terms look-up table and S-shape are used interchangeably throughout the text.
The suggestions for using dual-antenna setup and the limited look-up table are as follows:
1- Choose the APs positions in a way that limits the possibility of any movement in the regions from 0° to 30° and from 150° to 180°, so that all AoA estimates are unbiased by the estimator, and what will affect the estimation is the noise and the *channel condition parameters*.

2- Build the look-up table using a wider separation angle if it is not possible to choose the position of the AP as discussed in the previous point. Wider separation angle will give a wider range of unbiased AoA estimates, but still if TA is at an angle that is in the ambiguity region the bias in the estimated angle will be much larger than that of the 90° separation angle look-up table. As a result, if the AoA estimate is in the ambiguity regions, it is solved using advanced algorithms, or by using the time/phase information. The estimated AoAs are accurate in the linear region, and are less accurate in the ambiguity regions.
3- Use the dual-antenna setup in systems with more than one AP so that if TA is in the ambiguity region of one AP, it would be in the linear region of other APs. The aim is to use localization algorithms that give higher weights to to AoA estimates in the linear regions and lower weights to to those estimates that are in the ambiguous regions. In this way the additional APs could remedy the bias caused by TA being in the ambiguity region. However, the performance of the proposed estimator still suffers from the ambiguity region.
In this thesis, hard decision method using a look-up table was used for its simplicity and because off-line processing was used for positioning. This method can be used for on-line tracking as well, however, it is recommended to use more advanced methods such as particle filtering for better position estimations. In conclusion, AoA estimator performance for the dual-antenna setup will depend on the TA's location. The solution from the AoA estimates can be solved by using more than two antenna at the each AP that will result in more combinations of the RSSI values from different antennas, and this solution will be explained in the next section.

2.3.2 Four-Antenna Setup

As it was suggested in the previous section, the use of more than two antennas at each AP will improve AoA estimation. In this section a four-antenna setup is considered. The four-antenna setup will have six combinations between the RSSI values coming from the four antennas. The separation angle between each consecutive pair of antennas will be half the separation angle between the first antenna and the third antenna, and the separation angle between the second antenna and the fourth antenna. The separation angle between the first antenna and the fourth antenna will be three times the separation angle between the consecutive antennas separation angle. This will result in three look-up tables that are generated according to the corresponding separation angle. These look-up tables will estimate the AoA at a center point that have a different axis than that of the local axis of the AP. So the conversions between these axes are critical for calibrating the estimated AoA from the corresponding combination to the local axis of the AP. The proposed technique in this section will be referred to as "AoA Sections Estimator". Depending on the geometry of the antenna setup different sections are defined according to the best AoA estimate from different ΔRSSI combinations. Best AoA estimate is defined as the estimated AoA in the linear region of the look-up table, and this will ignore ambiguity region estimates; this will solve the dual-antenna setup estimation errors arising from the the ambiguity regions.
Figure 2.6 shows the orientations of the four antennas at the AP, where the first

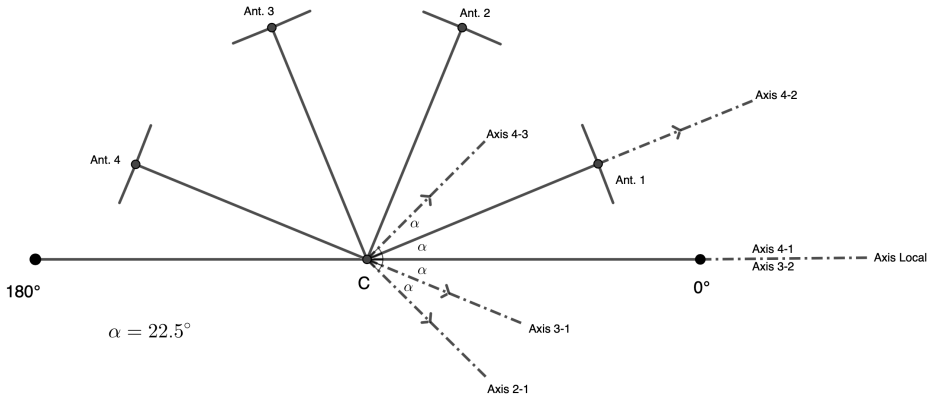

Figure 2.6: four-Antenna Setup.

antenna is oriented at 22.5°, the second antenna is oriented at 67.5°, the third antenna is oriented at 112.5°, and the fourth antenna is oriented at 157.5° from the reference axis of the AP. Sector 1 is defined as the sector where antenna 1 receives the highest RSSI value and the difference between the RSSI value between antenna 1 and antenna 2 is larger than 9 dB. The 9 dB will depend on the maximum gain of the antenna radiation pattern. The AoA will be estimated according to the look-up table that is generated according to a separation angle of 45° and the difference between RSSI value is taken between RSSI value from antennas 2 and 1. The estimated AoA will be in the region between 30° and 60°, and this will give the best possible AoA estimation. The estimated AoA should be calibrated to the reference axis of the AP by subtracting 45° from the estimated AoA.
Sector 2 is defined as the sector where antenna 2 receives the highest RSSI value, and the difference between RSSI value from antenna 2 is larger than that of antenna 1 and it is smaller that 9 dB. The AoA will be estimated according to the 90° look-up table and the difference of RSSI values is taken between antenna 3 and antenna 1, so that the estimated AoA will be in the region between 60° and 120°, which belongs to linear region. 22.5° will be subtracted from the estimated AoA in order to calibrate it to the reference axis of the AP.
Sector 3 is defined as the sector where antenna 2 receives the highest RSSI value and the difference between the RSSI value from antenna 2 and antenna 1 is larger than 9 dB and the difference between RSSI value from antenna 2 and antenna 3 is smaller 9 dB. The RSSI difference will be taken between antenna 3 and antenna 2, and the estimated AoA will be taken from the 45° look-up table. The estimated AoA will be in the region between 60° and 120°, that belongs to the linear region of the look-up table. There is no calibration needed for this AoA estimate, as the AoA estimate is already calibrated to the reference axis of the AP.
Sector 4 is defined as the sector where antenna 3 receives the highest RSSI value, and the difference between the RSSI value from antenna 3 and RSSI value from antenna 2 is smaller than 9 dB and the RSSI value from antenna 3 is larger than 9

dB than that of antenna 4. The 90° look-up table will be used for estimating AoA and the ΔRSSI value will be calculated using the RSSI values from antenna 4 and antenna 2. The estimated AoA will be in the region between 60° and 120°, that belongs to the linear region of the look-up table. To calibrate the estimated AoA to the reference axis of the AP, 22.5° is added to to the estimated AoA. Sector 5 is defined as the sector where antenna 4 receives the highest RSSI value, and the difference between the RSSI value from antenna 4 and antenna 3 is smaller than 9 dB. The RSSI difference will be taken between the RSSI values from antenna 4 and antenna 3, and this difference will be used in the 45° look-up table in order to estimate the AoA. The AoA estimate will be in the linear region and ranging from 60° to 120°. 45° will be added to the estimated AoA in order to calibrate the AoA to the reference axis of the AP. Sector 6 is defined as the sector where antenna 4 receives the highest RSSI value and the difference between RSSI values from antenna 4 and antenna 3 is larger than 9 dB. The RSSI difference between RSSI values from antenna 4 and antenna 2 will be used in the 90° look-up table in order to estimate the AoA. The AoA estimate will be between 30° and 60°, and there is no need for calibration to the reference axis of the antenna.
An AoA sector estimator is a straight forward approach that is device friendly, time efficient, and do not demand complex operations. The only thing needed for this approach are the 4 RSSI values from the four antennas at the same time instance, the predefined sectors that depends on the maximum gain of the radiation pattern of the antennas used, and two look-up tables that are generated for the two chosen separation angles of 45^o and 90^o.
the four-antenna setup and AoA sectors estimator can work as a stand alone system as the AoA estimation are highly accurate. However, this setup works only for the cases where TA is in the regions from 0° to 180°. It is recommended to direct the four antennas to the aimed region of estimation so that the center of the aimed region of estimation is exactly between antenna 3 and antenna 2. To be able to estimate all angles between from 0° to 359°, the four antennas can be placed 90^o separated from each other; in this case only one look-up table is needed for AoA estimation and only four sectors need to be defined with less conditions than those of the proposed approach. A drawback of such setup is that only RSSI difference between consecutive antennas can be used since the assumptions used to generate the look-up tables does not apply for other antennas. It is recommended to use a circular equidistant 8-antennas setup to estimate AoAs from 0° to 359°. The reason is having more combination between eight RSSI values would improve the angular accuracy.

AoA sector estimator provided a simple solution for the highly accurate AoA estimates, and solved the ambiguity issues that were present for the dual antenna approach. There are many other techniques that can be used instead of the AoA sector estimator, that can enhance the angular accuracy, but due to time constrains the authors prioritised measurement testing and system design over investigating other techniques that can provide a joint AoA estimate from all the available information from the antennas.

Chapter 3

Combined AoA-RSSI position Estimation

In this section RSS and AoA observation models are introduced and the localization problem is formulated in a two-dimensional space. Let $\boldsymbol{x}$ be the unknown location of the TA, and $\boldsymbol{a_i}$ be the known location of the i-th AP with $i = 1, \ldots, N$. In Figure 3.1, $\boldsymbol{x} = [x_x,\, x_y]^T$ denotes the true coordinate of the TA and $\boldsymbol{a_i} = [a_{i,x},\, a_{i,y}]^T$ denotes the true location of the i-th AP. While d_i and ϕ_i represent the distance and the angle between the TA and i-th AP. Then, the noise free received power from the TA and the i-th AP can be calculated as [18]:

$$P_{RX,i} = P_{TX}\, G_{TX}\, G_{RX,i} \left(\frac{\lambda}{4\,\pi\, d_i}\right)^2, \qquad for \quad i = 1, \ldots, N \tag{3.1}$$

where, $P_{RX,i}$ is the received power at the i-th AP, P_{TX} and G_{TX} are the transmitted power and the gain of the transmitter respectively, $G_{RX,i}$ is the gain of the i-th AP, λ is the wavelength of the transmitted signal and is given by $\lambda = \frac{Speed of light}{signal frequency}$ and d_i is the distance from TA to the i-th AP. The above equation in dB form is given as:

$$P_{RX,i} = P_{TX} + G_{TX} + G_{RX,i} + 20\, \log\left(\frac{\lambda}{4\,\pi\, d_i}\right), \tag{3.2}$$

or to better point out the distance dependence, it is advantageous to first compute the received power at a distance of 1 m. Then, the above equation can be rewritten as:

$$P_{RX,i} = P_{RX}(1\,\mathrm{m}) - 20\, \log\big(d_i\big), \tag{3.3}$$

and the received power at 1 m is given by:

$$P_{RX}(1\,\mathrm{m}) = P_{TX} + G_{TX} + G_{RX,i} + 20\, \log\left(\frac{\lambda}{4\,\pi\,.\,1}\right). \tag{3.4}$$

In the presence of noise, $P_{RX,i}$ can be written as:

$$P_{RX,i} = P_{RX}(1\,\mathrm{m}) - 10\,\eta\, \log\big(d_i\big) + w_i\,, \qquad for \quad i = 1, \ldots, N \tag{3.5}$$

where $w_i \sim \mathcal{N}(0,\, \sigma^2_{w_i})$ is the log-normal shadowing term modeled as a zero-mean Gaussian random variable with standard deviation σ_{w_i} (dB).

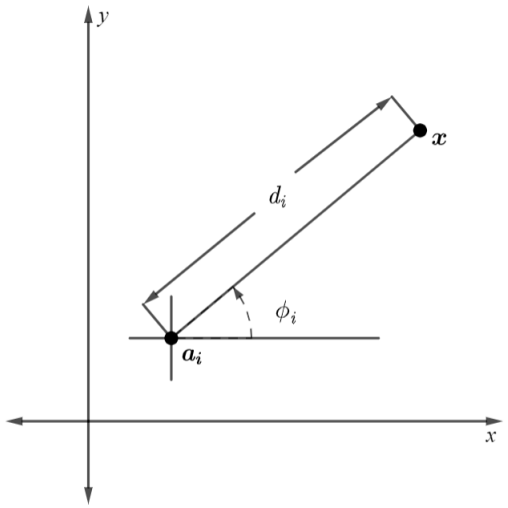

Figure 3.1: Graphical illustration of the measurement models in a two-dimensional space.

The angle of arrival, as described in the previous chapter, can be obtained by implementing a directional antenna [19]. By using simple geometry, the azimuth angle is modeled as:

$$\phi_i = \tan^{-1}\left(\frac{x_y - a_{i,y}}{x_x - a_{i,x}}\right) + m_i\,, \qquad for \quad i = 1, \ldots, N \tag{3.6}$$

Where $m_i \sim \mathcal{N}(0,\, \sigma^2_{m_i})$ is a zero-mean Gaussian random variable with standard deviation σ_{m_i} (rad). Then by defining an observation vector $\boldsymbol{\theta} = [\boldsymbol{P}^T,\, \boldsymbol{\phi}^T]^T$ where $\boldsymbol{P} = [P_{RX,i}]$ and $\boldsymbol{\phi} = [\phi_i]$, the conditional probability density function can be written as:

$$p(\boldsymbol{\theta}|\boldsymbol{x}) = \prod_{i=1}^{2N} \frac{1}{\sqrt{2\,\pi\sigma_i^2}}\, \exp\left\{ -\frac{\big(\theta_i - f_i(\boldsymbol{x})\big)^2}{2\,\sigma_i^2}\right\}, \tag{3.7}$$

where $\boldsymbol{\sigma}_i = [\sigma_{w_i},\, \sigma_{m_i}]^T$ and $\boldsymbol{f(x)} = \left[P_{RX}(1m) - 10\eta\log(d_i), \quad \tan^{-1}\left(\frac{x_y - a_{i,y}}{x_x - a_{i,x}}\right)\right]^T$.

3.1 Linear Least Square (LLS) Postion Estimator

The authors in [20] formulated the Linear Least Square (LLS) solution to the localization problem as:

$$\hat{\mathbf{u}}_{\mathrm{LLS}} = \boldsymbol{A}^{\dagger}\hat{\boldsymbol{b}}, \tag{3.8}$$

where $\boldsymbol{A}^{\dagger}$ is the Moore-Penrose pseudo-inverse of the matrix $\boldsymbol{A}$ and is given by $\boldsymbol{A}^{\dagger} = (\boldsymbol{A}^T\boldsymbol{A})^{-1}\boldsymbol{A}^T$ and the matrix $\boldsymbol{A}$ is given by:

$$\boldsymbol{A} = \begin{bmatrix} \boldsymbol{e}_N & \boldsymbol{0}_N \\ \boldsymbol{0}_N & \boldsymbol{e}_N \end{bmatrix} \qquad \in \mathbb{R}^{2\text{x}1}, \tag{3.9}$$

where N is number of pairs of BL beacons i.e. APs, $\boldsymbol{e}_N$ and $\boldsymbol{0}_N$ denote column vectors of N ones and zeros, respectively. Likewise,

$$\hat{\boldsymbol{b}} = [\hat{\boldsymbol{b}}(x), \hat{\boldsymbol{b}}(y)]^T \qquad \in \mathbb{R}^{2N\text{x}1}, \tag{3.10}$$

where

$$\hat{\boldsymbol{b}}(x) = \begin{bmatrix} x_1 + \hat{d}_1 \cos(\hat{\theta}_1)\,\delta_1 \\ \vdots \\ x_N + \hat{d}_N \cos(\hat{\theta}_N)\,\delta_N \end{bmatrix} \qquad \in \mathbb{R}^{N\text{x}1}, \tag{3.11}$$

and

$$\hat{\boldsymbol{b}}(y) = \begin{bmatrix} y_1 + \hat{d}_1 \sin(\hat{\theta}_1)\,\delta_1 \\ \vdots \\ y_N + \hat{d}_N \sin(\hat{\theta}_N)\,\delta_N \end{bmatrix} \qquad \in \mathbb{R}^{N\text{x}1}. \tag{3.12}$$

In Equation (3.12), x_i and y_i are the known coordinates of the center point of the i-th AP, $\hat{d}_i$ and $\hat{\theta}_i$ are the estimated distance to the center point of the i-th AP and the estimated AoA on the center point of the i-th AP, and δ_i is an unbiasing constant for AoA-RSS signal and is given by:

$$\delta_i = \exp\left(\frac{\sigma_{m_i}^2}{2} - \frac{\sigma_{w_i}^2}{2(\gamma\,\eta_i)^2}\right), \tag{3.13}$$

where $m_i \sim \mathcal{N}(0, \sigma_{w_i}^2)$ represents the zero mean Gaussian noise in the angle estimate and $w_i \sim \mathcal{N}(0, \sigma_{w_i}^2)$ is the zero mean Gaussian noise random variable characterizing the shadowing effects. $\gamma = \frac{10}{10\ln(10)}$ and η_i is the PLE associated with i-th AP.

3.2 Least Square (LS) Postion Estimator

Theoretically, the performance of the LLS estimator can be improved by introducing weights into the solution given by the LLS estimator; where APs estimated to be further away from the TA are given lower weights than APs estimated to be closer to the TA [6]. Then the solution to the Least Square (LS) estimator is given by

$$\hat{\mathbf{u}}_{\text{LS}} = \left(\boldsymbol{A}^T\boldsymbol{W}\boldsymbol{A}\right)^{-1}\boldsymbol{A}^T\boldsymbol{W}\hat{\boldsymbol{b}}. \tag{3.14}$$

Where $\boldsymbol{A}$ and $\hat{\boldsymbol{b}}$ are given by 3.9 and 3.10 respectively. Whereas, the weight matrix $\boldsymbol{W}$ is given by:

$$\boldsymbol{W} = \text{diag}\big[\sqrt{w_1}, \ldots, \sqrt{w_N}, \ldots \sqrt{w_1}, \ldots, \sqrt{w_N}\,\big] \qquad \in \mathbb{R}^{2N\text{x}2N}, \tag{3.15}$$

and w_i is given by:

$$w_i = 1 - \frac{\hat{d}_i}{\sum_{i=1}^{N} \hat{d}_i}. \tag{3.16}$$

Introduction of these weights is motivated by Figure 3.2. Here it can be seen that an error in angle estimation results in larger position estimation error at larger distances compared to at smaller distances.

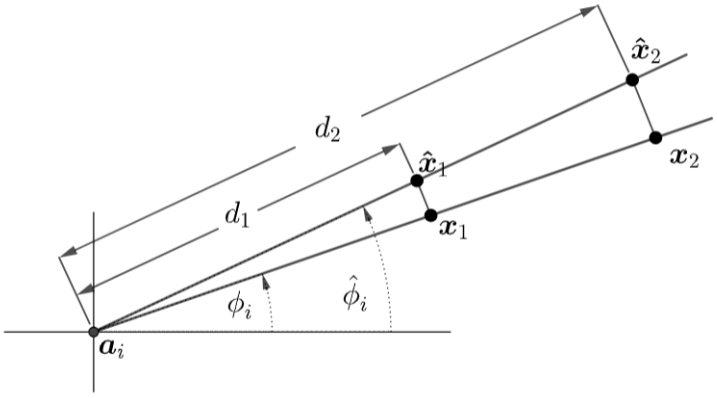

Figure 3.2: Illustration of azimuth angle estimation error at different distances.

3.3 Weighted Linear Least Square (WLLS) Postion Estimator

The solution to the localization problem given by the LS estimator can be improved by utilizing the communication link quality between the TA and APs. This means that links with larger noise are given small weights and links with small noise are given larger weights [20], [6]. As per [20], the link quality is given by the covariance matrix $\boldsymbol{C}$ where

$$\boldsymbol{C} = \begin{bmatrix} \boldsymbol{C}(xx) & \boldsymbol{C}(xy) \\ \boldsymbol{C}(xy) & \boldsymbol{C}(yy) \end{bmatrix} \qquad \in \mathbb{R}^{2N\text{x}2N} \tag{3.17}$$

and the sub-matrices of Equation (3.17) reduces to 0 for i≠j and to Equations (3.18)-(3.20) for i=j.

$$\boldsymbol{C}(xx)_{i,i} = \frac{d_i^2}{2}\,\kappa_i + \frac{d_i^2}{2}\,\cos\left(2\theta_i\right)\bar{\kappa_i} - \left(d_i\,\cos\left(\theta_i\right)\right)^2 \tag{3.18}$$

$$\boldsymbol{C}(yy)_{i,i} = \frac{d_i^2}{2}\,\kappa_i - \frac{d_i^2}{2}\,\cos\left(2\theta_i\right)\bar{\kappa_i} - \left(d_i\,\sin\left(\theta_i\right)\right)^2 \tag{3.19}$$

$$\boldsymbol{C}(xy)_{i,i} = d_i^2\,\cos\left(\theta_i\right)\sin\left(\theta_i\right)(\bar{\kappa_i} - 1) \tag{3.20}$$

where $\kappa_i = \exp\left(\frac{\sigma_{w_i}^2}{2(\gamma\,\eta_i)^2} + \sigma_{m_i}^2\right)$, $\bar{\kappa_i} = \exp\left(\frac{\sigma_{w_i}^2}{2(\gamma\,\eta_i)^2} - \sigma_{m_i}^2\right)$, and the notation $\boldsymbol{T}_{i,j}$ refers to the element of the matrix $\boldsymbol{C}$ at the i-th row and j-th column. The Weighted Linear Least Square (WLLS) solution is then obtained by:

$$\hat{\mathbf{u}}_{\text{WLLS}} = \left(\boldsymbol{A}^T\boldsymbol{C}^{-1}\boldsymbol{A}\right)^{-1}\boldsymbol{A}^T\boldsymbol{C}^{-1}\hat{\boldsymbol{b}} \tag{3.21}$$

3.4 Comparison/Motivation of Proposed Postion Estimators

The Maximum Likelihood, ML, estimate, $\hat{\boldsymbol{x}}$, of the location of the target can be obtained by maximizing the log of the likelihood function given in Equation (3.7) with respect to $\boldsymbol{x}$ [21] as:

$$\hat{\boldsymbol{x}} = \arg\min_{\boldsymbol{x}} \sum_{i=1}^{2N} \frac{1}{\sigma_i^2}[\theta_i - f_i(\boldsymbol{x})]^2 \quad . \tag{3.22}$$

However the above estimator is highly non-convex and its solution cannot be obtained in a closed-form. The authors in [6] showed that it is possible to approximate the ML estimator by other estimators that are less complex. Three of those estimators are: LLS, LS, and WLLS which were introduced earlier in this chapter. A second motivation behind choosing these estimators is that only information about RSSI and AoA are needed to find a solution to the localization problem. RSSI is readily available on many commercial radio devices [22] while AoA can be obtained from ΔRSSI using the proposed technique in Chapter 2 of this thesis.

Chapter 4

BLE System

4.1 BLE Overview

Bluetooth

Bluetooth is a wireless technology standard used to transfer data over short distances between fixed and/or mobile devices in the Industrial, Scientific, and Medical (ISM) radio band, from 2.400 GHz to 2.485 GHz and is managed by Bluetooth Special Interest Group, SIG. The development of a "short-link" radio technology which later was named Bluetooth started in early 1990's. By 1999, the Bluetooth Specification 1.0 Basic Rate (BR) was released and the first consumer Bluetooth device, a hand free mobile headset, was launched. In 2002, Bluetooth was standardized by the Institute of Electrical and Electronics Engineers (IEEE) as IEEE 802.15.1. In 2004, SIG adopted the Core Specification 2.0 Enhanced Data Rate (EDR). In 2010, Bluetooth SIG announced adoption of Bluetooth Core Specification 4.0 with low energy technology which is known as BLE [11]. Bluetooth technology is optimized for continuous data streaming at ISM bands which are reserved internationally for industrial, scientific, and medical purposes. The technology uses 79 channels at frequencies 2.402-2.480 GHz with 1 MHz spacing and uses Frequency-Hopping Spread Spectrum (FHSS) to flip between these channels. It uses three different modulation techniques: GFSK, $\pi/4$-DQPSK, and 8DPSK with a data rate that ranges between 1 Mbit/s to 3 Mbit/s depending on which modulation is used. See Table 4.1.

Bluetooth Low Energy (BLE)

BLE is a Wireless Personal Area Network (WPAN) that uses the ISM bands for data transmission; it is designed for reduced energy consumption and cost while maintaining similar communication range compared to classic Bluetooth, BR/EDR. BLE uses Gaussian Frequency Shift Keying (GFSK) modulation and achieves data rates from 125 Kbit/s to 2 Mbit/s with power consumption as low as one half to one hundredth of classical Bluetooth. In addition to point-to-point communication that is used in classical Bluetooth, BLE can be used to broadcast, and for mesh communication. In contrast to classic Bluetooth that uses 79 channels with 1 MHz spacing, BLE uses 40 channels with a spacing of 2 MHz from 2.400 GHz to 2.485 GHz, see Figure 4.2. A note about BLE is that it is a connection

	BLE	BR/EDR
Optimize For	Short Burst Data Transmission	Continuous Data Transmission
Frequency Band	2.4 GHz ISM Band (2.402 GHz ∼ 2.480 GHz)	2.4 GHz ISM Band (2.402 GHz ∼ 2.480 GHz)
Channels	40 Channels With 2 MHz Spacing (3 Advertising and 37 data) Channels	79 Channels With 1 MHz Spacing
Channel Usage	Frequency-Hopping Spread Spectrum (FHSS)	Frequency-Hopping Spread Spectrum (FHSS)
Modulation	GFSK	GFSK, $\pi/4$-DQPSK, 8-DPSK
Power Consumbtion	∼ 0.001x to 0.5x of Reference Value	1 (Reference Value)
Data Rate	125 kbps ∼ 2 Mbps	BR(GFSK): 1 Mbit/s EDR($\pi/4$-DQPSK): 2 Mbit/s EDR(8-DPSK): 3 Mbit/s
Max. TX Power	Class 1: 100 mW(20 dBm) Class 1.5: 10 mW (10 dBm) Class 3: 2.5 mW (4 dBm) Class 4: 1 mW (0 dBm)	Class 1: 100 mW (20 dBm) Class 3: 2.5 mW (4 dBm) Class 4: 1 mW (0 dBm)
Network Topologies	Point to Point(Piconet Included) Broadcast Mesh	Point to Point(Piconet Included)
Voice Capable	No	Yes

Table 4.1: Comparison of BLE and classical Bluetooth

oriented wireless technology, i.e. devices that want to exchange data must establish a connection before data transmission is possible. To elaborate, a BLE device can be in one of five possible states as described in Figure 4.1. Devices are detected by a procedure that broadcasts packet in the "advertising" state. Devices in the advertising state can transmit connection-less data to scanning devices which are in "scanning" state. Advertising devices signalize scanning and initiating devices that it is ready for connection. The scanning device then responds to initiate a connection. Furthermore, devices in states "initiating" and "scanning" will listen for packets from specific advertising devices.

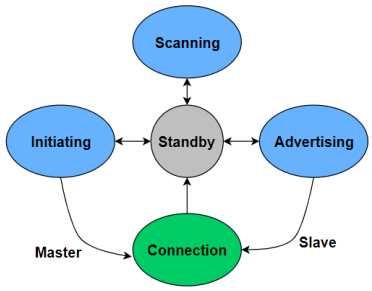

Figure 4.1: BLE channel usage in the ISM band.

A BLE device enters the "connection" state when a connection is established. Finally, a device is said to be in "standby" state if it is in none of the previous states. i.e. when it is not in connection state nor it is attempting to connect. Within the state "connection" a device will have one of two roles: if the device enters the connection from "initiating" it will have the "Master Role". On the other hand, if it enters connection from "advertising" state, it will have the "Slave Role" [23].

BLE Channels

As previously stated, a BLE device uses 40 channels/frequencies of 2 MHz spacing. Of the 40 channels, channels 37, 38, and 39 at frequencies 2402 MHz, 2426 MHz, and 2480 MHz, respectively [24] are dedicated for advertising while the other 37 channels are dedicated to data transmission, see Figure 4.2. The advertising device sends a packet on at least one of three channels periodically over an interval called advertising interval. Then, to reduce probability of multiple consecutive collisions, a random delay up to 10 milliseconds is added to the advertising interval.

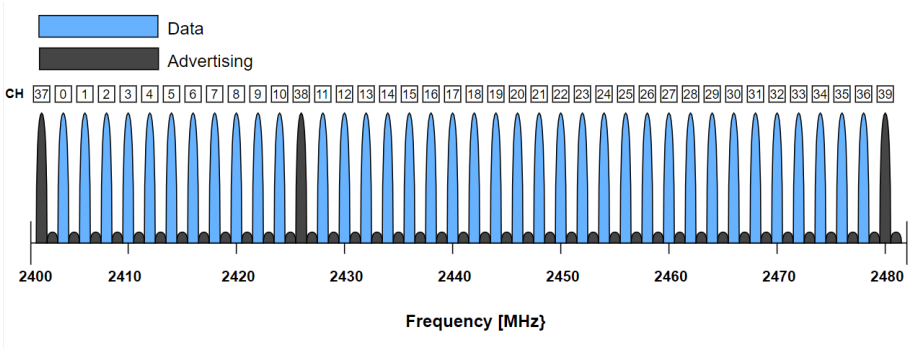

Figure 4.2: BLE channel usage in the ISM band.

Frequency Hopping

When connection is established, a frequency hopping scheme is applied to choose the channel to be used for next transmission from the available 37 data channels according to Equation (4.1):

$$f_{n+1} = (f_n + hop)\, mod 37 \tag{4.1}$$

where n is the current connection event, and hop is an arbitrary value that ranges from 5 to 16 and is generated when connection is established. This value is added to the current frequency value f_n modulo 37 to choose the frequency to be used at connection event $n + 1$.

Packet Type

BLE advertising channel packets and data channels packets have the same format. Each packet consists of a preamble followed by an access address and protocol data unit (PDU) and is ended with a CRC. As explained in Figure 4.3, the PDU part of the packet consists of a 2-bytes header and followed by a payload. For further reading about Bluetooth low energy packet format, the reader is referred to Bluetooth Core Specifications v5.1 vol. 6, part B, section 2 [25].

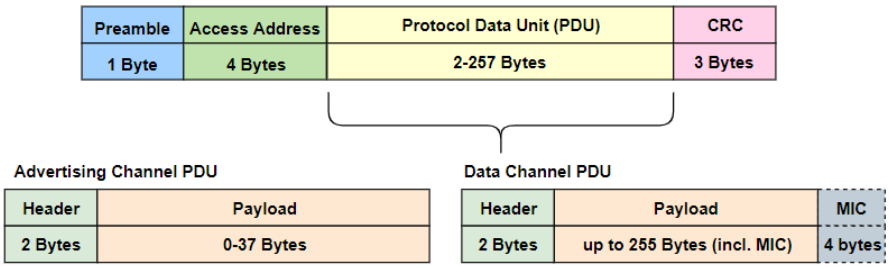

Figure 4.3: BLE packet format as per core specification v5.1 [25].

Bluetooth Low Energy Discovery Process

In BLE, advertising channels are used for the advertiser and scanner to find each other [26]. Advertising channels in BLE are explained in the BLE Channels section. Each time the device advertises, same packet is transmitted in each of the three advertising channels. This sequence of events is defined as the advertising event. These advertising events can be transmitted as frequent as 20 milliseconds to as infrequent as 10.24 seconds. To prevent overlapping of advertising events from multiple devices, a random time interval up to 10 milliseconds is added between advertising events. Figure 4.4 shows the discovery process, so that synchronization between the advertiser and the scanner is not demanded. The scanner listens to only one channel, while the advertiser is transmitting on the three frequency channel within a time interval that is less than that of the scanner. While the scanner is listening to one of the channels the maximum number of detected packets depends on the scanning interval. The example in Figure 4.4 (inspired by [26]) shows the procedure for detection for a scanning interval of 50 ms and a scanning window of 25ms, where the scanning interval defines the time needed for the scanner to flip from one channel to the another,while the scanning window defines the time the scanner is listening on that frequency channel within the scanning interval . The maximum number of detected packet in this example was two. For the setup

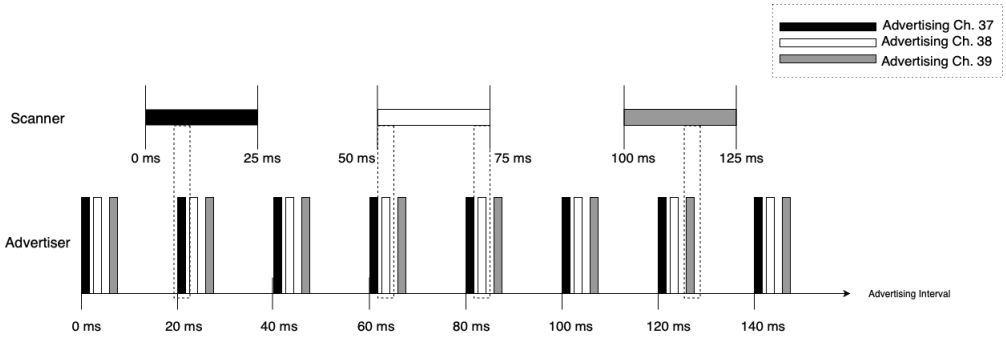

Figure 4.4: Advertising & Scanning.

that is utilized in this project, the gateway acted as the scanner, while the tag was acting as the advertiser. The tag was configured to transmit at the maximum allowed advertising interval of 100 ms, while the BLE gateway scanning interval and the corresponding scanning window were not defined. For that thousands of received packet es were logged from the gateway, and the difference between the times for consecutive packets was ranging between 100 ms and 300 ms. The conclusion of this small test showed that within the 1 s interval the scanner should be able listen to all the frequency channels. The information about the scanning interval and the scanning window is crucial for the averaging process, so that with the 1s the maximum number of packet that can be received is 10 packets with a guarantee that a packet at least from each frequency channel was received.

4.2 Hardware

The equipment used for BLE measurement consisted of: A BLE proximity beacon, BlueBeacon Maxi, hereon, TA along with two BLE beacon reader, BlueBeacon Gateway, hereone, Gateway both manufactured by BlueUp S.r.l.s, and two dual band directional patch antennas, W24-58-CP-9 manufactured by Panorama Antennas Ltd.

4.2.1 BlueBeacon Maxi

The beacon is battery powered that supports advertising multiple frames with iBeacon, Eddystone, and/or Quuppa format with transmitting power of -20 to 4 dBm and an advertising interval of 100 ms to 5 s with radio specifications that are according to Bluetooth 4.0. The beacon is equipped with a PIFA antenna with a maximum gain of 2 dB and according to the manufacturer it produces an omnidirectional pattern. However, when used in the field conducting real measurements it was noticed that despite the claim of omnidirectionality, the real pattern of this beacon is not omnidirectional and a change of its orientation, in fact, affects the received power drastically at the receiver. The physical appearance of the TA is shown in Figure 4.5

Figure 4.5: Physical appearance of BlueBeacon Maxi.

4.2.2 BlueBeacon Gateway

This BLE reader is capable of reading and identify the beacons in range and make the readings available to the user(s). The collected data from TA can be either collected and averages over one second and then pushed to a server or be available as a RESTful API. The former approach is not useful for the purpose of this thesis since averaging costs us valuable information needed in finding channel statistics that will be explained in a later chapter. The second approach had it shortcomings as well since the only way to get the data was to request it using HTTP request; we were restricted by the hardware and hence, continuous data collection over a longer period was not possible since it required processing capabilities that was beyond the available PCs used for this thesis. A way around this is program the gateways to push the data to an allocated server. However, this was not possible due to time restrictions.

Figure 4.6: Physical appearance of BlueBeacon Gateway.

4.2.3 Panorama Patch Antenna

The W24-58-CP-9 directional antenna comes in an enclosure with dimensions 93mm x 93mm x 25mm and has a peak gain of 9 dBi with a 3dB beam-width of 60° at 2.4 GHz. The physical appearance of the enclosure can be seen in Figure 4.7 and its pattern is depicted in Figure 4.8 [27].

Figure 4.7: Physical appearance of Panorama W24-58-CP-9 directional antenna.

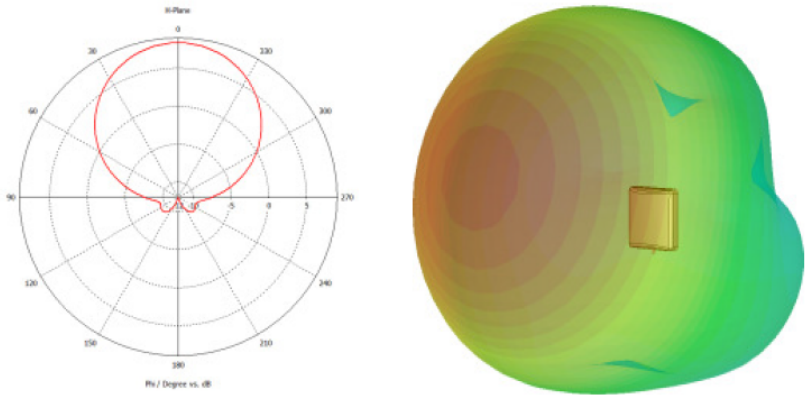

Figure 4.8: Depiction of Panorama W24-58-CP-9 directional antenna pattern as given by the manufacturer [27].

4.3 Estimation of Channel Statistics

To prepare for localization experiment, preliminary measurements were conducted to explore the area of measurement and to find channel statistics that will be needed for the positioning algorithm. As a first step, a flat area free of obstacles was selected to ensure LoS conditions. Figure 4.9 is a depiction of the measurement location and the area bordered by the black square represents where the measurements took place. The channel measurement involved using one AP equipped with two directional antennas, $r1$ and $r2$, with a c2c distance equal to L, the wavelength of the transmitted signal. Each of $r1$ and $r2$ were L_c away from a center point C with $r1$ and $r2$ directed β_c clockwise from angle 180° and β_c anticlockwise from angle 0° respectively on the local coordinate of the AP. Center of measurement area was ensured to be perpendicular on the local x-axis of the AP at point C, see Figure 4.10. In this configuration, L_c was equal to 8.7 cm, L was 12.3 cm and β_c was 45°.

Three different type of measurements were conducted; in the first measurement, RSSI values were collected moving at a constant speed along an arc, from 0° to 180° at different distances from the AP, hereon referred to as "angular measurement". See Figure 4.11. While in the second measurement, RSSI values were collected moving along a constant angle away from AP up to 20 m and then moving back towards the AP. This measurement will, hereon, be referred to as "distance measurement". see Figure 4.16. Finally, in third set of measurements, RSSI values at predefined points on the map, hereon, "static measurement" were collected for further analysis; these points can be seen in Figure 4.33. The statistics obtained from these measurements are discussed in next subsections.

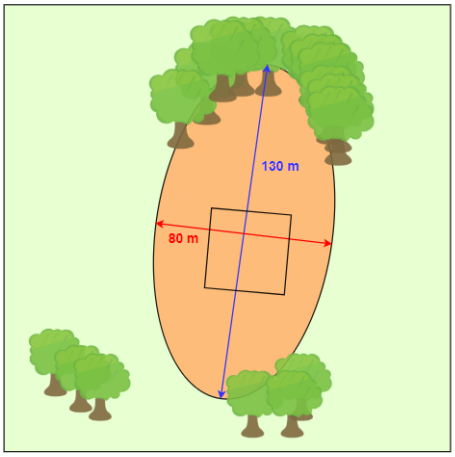

Figure 4.9: Depiction of measurement area.

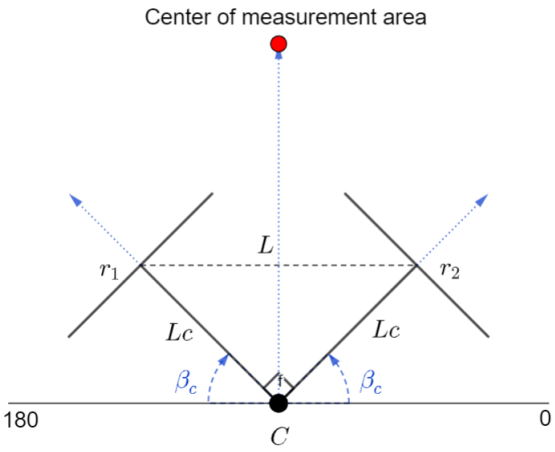

Figure 4.10: Orientation of the two antennas at the access point.

4.3.1 Angular Measurement

The purpose of this measurement was to analyze the behavior of ΔRSSI at different distances when $\phi \in [0, 180°]$. In theory, as ϕ increases from 0 to 180°, ΔRSSI follows a S-shaped curve as was discussed in Chapter 2.3.
Here, analysis was done when TA was moved at a constant speed from 0 to 180° at distances 1 m, 5 m, and 10 m away from AP. Figure 4.11. This measurement was done for different angle of separations between r_1 and r_2. Results from different configurations are shown below.
Looking at Figures 4.12 and 4.13, it can be observed that ΔRSSI values from the measurement are in agreement with our expectation from the theoretical part.

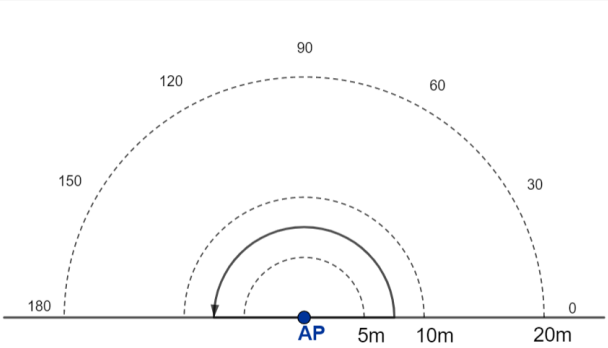

Figure 4.11: Arc movement at different distances around AP.

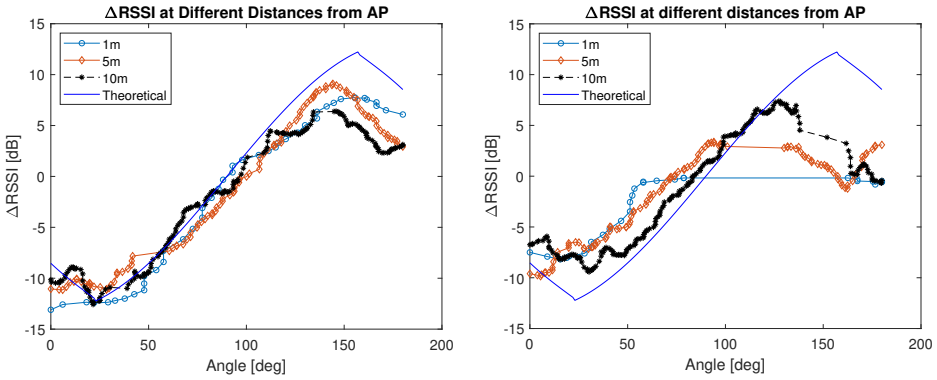

(a) ΔRSSI when $\beta = 45°$, center-to-center separation $= \lambda$.

(b) ΔRSSI when $\beta = 45°$, center-to-center separation $= \frac{3}{4}\lambda$.

Figure 4.12: ΔRSSI when $\beta = 45°$ with different center-to-center configurations.

Albeit, there are two points that need to elaborated on. First, in Figure 4.12b, there are gaps in the readings on the right side of the plot. The reason behind this behaviour is hardware related. To collect RSSI information from the gateways, "RESTful API GET" method was used to request data from the gateways. Continuous use of "RESTful API GET", however, reduced the performance of computers used in this experiment. A more convenient way to collect these information is to connect the gateways to dedicated servers and have them push the data as soon as they are received to ensure that all data are collected. Note that the measured data are compared to synthetically generated patterns and this could add a bias that affects all the results in this chapter. It is recommended to measure the actual patterns in an anechoic chamber. The second point is the behaviour of RSSI difference when the angle of separation was 90° at 1 m away from the AP, see Figure 4.13a.

To study the behaviour of the curve at close ranges to the AP, further analysis was

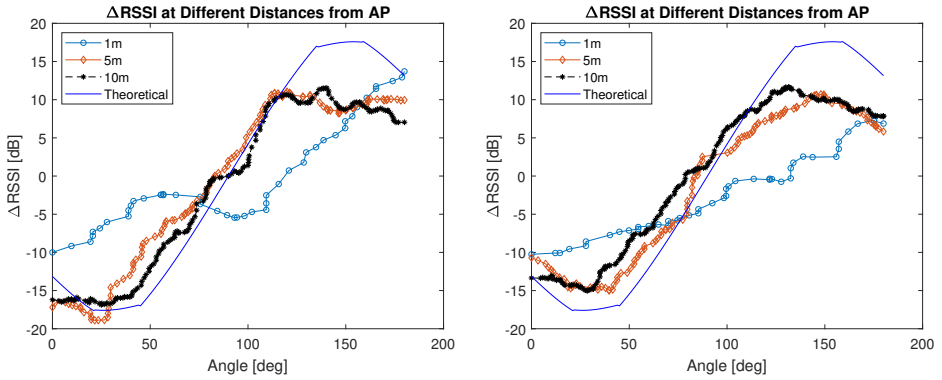

(a) ΔRSSI when $\beta = 90°$, center-to-center separation $= \lambda$. **(b)** ΔRSSI when $\beta = 90°$, center-to-center separation $= \frac{3}{4}\lambda$.

Figure 4.13: ΔRSSI when $\beta = 90°$ with different center-to-center configurations.

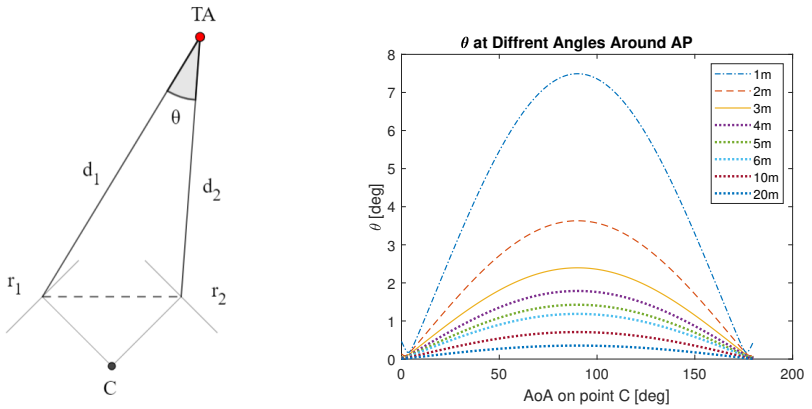

(a) Angle difference, θ, experienced by r_1 and r_2. **(b)** Values of theta θ at different distances.

Figure 4.14: Effect of close proximity to the access point on θ.

performed to determine the cause of such behaviour. The technique used in this project is based on the assumption that, effectively, r_1 and r_2 are located on the same point i.e. The c2c separation is negligible and the angle θ shown in Figure 4.14a is equal to effectively zero. This assumption holds for higher ranges, but at close ranges such the one under consideration it might not; from Figure 4.15b it can be observed that the value of θ ranges from 0 to 7°. It was found that the effective angle of separation at 1 m varies between 89° to 97°, Figure 4.15b, but it does not impact the S-shape in a way that could explain the behaviour witnessed in 4.13a. See Figure 4.15b.

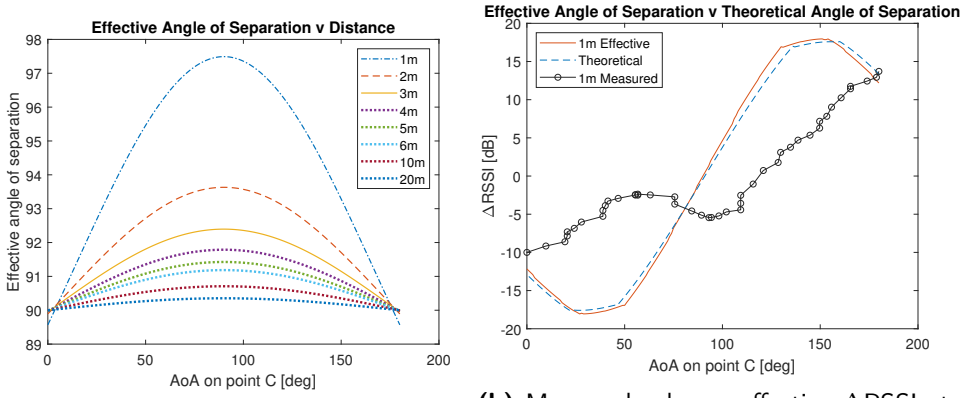

(a) Effective angle of separation.

(b) Measured values v effective ΔRSSI at 1 m and theoretical values.

Figure 4.15: Effective angle of separation and RSSI difference.

4.3.2 Distance Measurement

The aim in this measurement was to estimate the channel PLE, η, and deviations in ΔRSSI. The TA was moving away from the AP from 1 m to 20 m and then moving back towards the AP at a constant speed. Movement was at fixed angles, α on the local coordinate of the AP as seen in Figure 4.16.

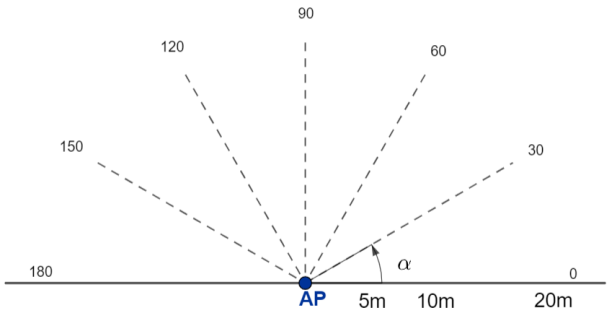

Figure 4.16: Movement along constant angle.

Figures 4.17 to 4.29 display the results obtained from the measurements. In these figures, ΔRSSI values were measured and compared to the expected values at each angle of interest. At each figure, the measured values are plotted against the expected value in the plots on the left while the Probability Density Function (PDF) of the deviation from the expected value is shown in the plots on the right. The PDF plots are divided into three plots; top left plot corresponds to movements away from the AP, bottom left corresponds to the movement towards the AP, and the plot on the right displays the combination of both movements. From Figures 4.17, 4.18, 4.20, and 4.21 it is observed that at angles 0°, 15°, 45°, and 60°,

there was a change in measured ΔRSSI values; this behaviour, however, was not observed in the rest of angles under study. This behaviour could be contributed to the surrounding environment.

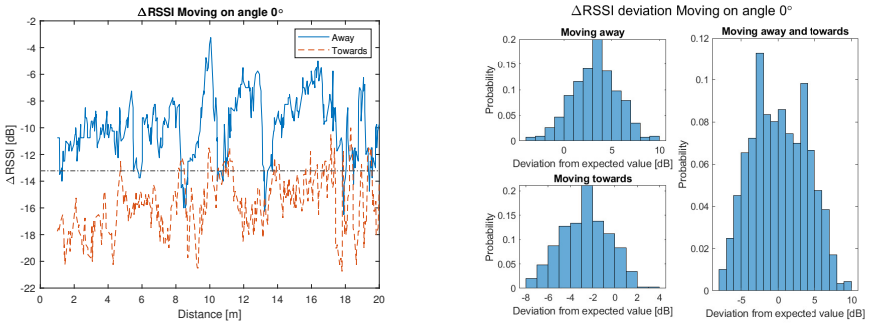

(a) Measured ΔRSSI compared with expected value

(b) Deviation of measured ΔRSSI from the expected value at the angle of interest

Figure 4.17: Movement along angle 0° on the point C

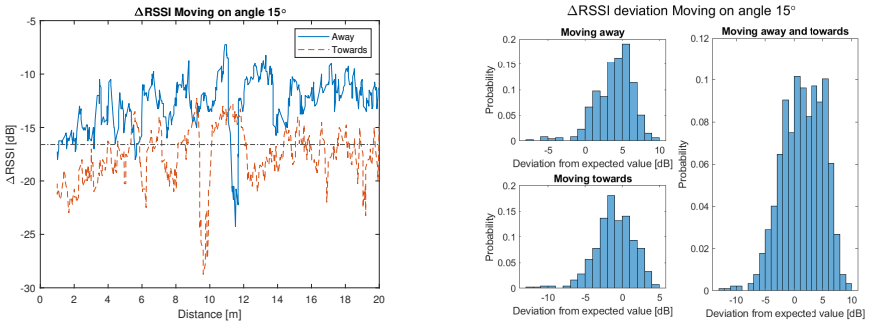

(a) Measured ΔRSSI compared with expected value

(b) Deviation of measured ΔRSSI from the expected value at the angle of interest

Figure 4.18: Movement along angle 15° on the point C

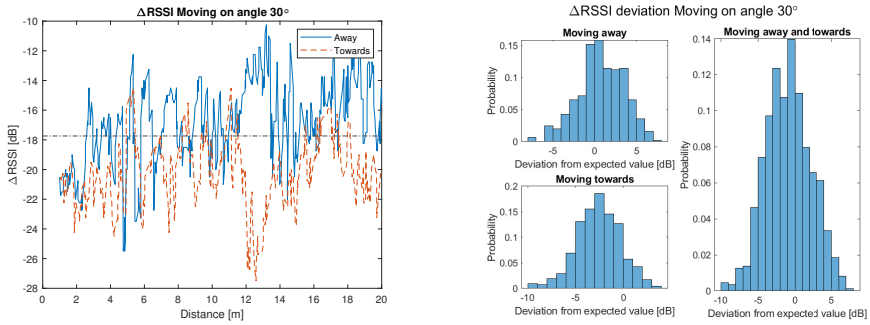

(a) Measured ΔRSSI compared with expected value

(b) Deviation of measured ΔRSSI from the expected value at the angle of interest

Figure 4.19: Movement along angle 30° on the point C

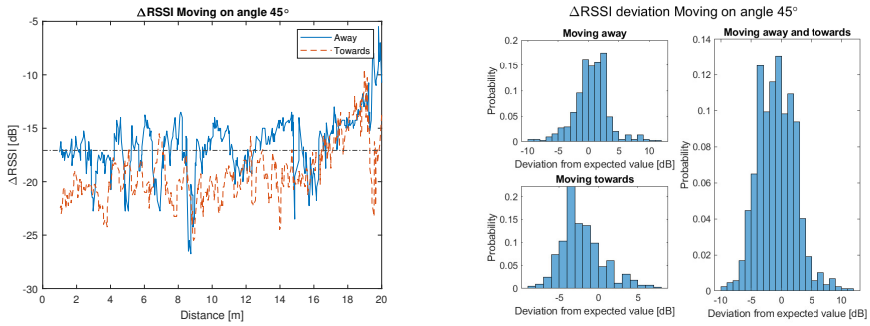

(a) Measured ΔRSSI compared with expected value

(b) Deviation of measured ΔRSSI from the expected value at the angle of interest

Figure 4.20: Movement along angle 45° on the point C

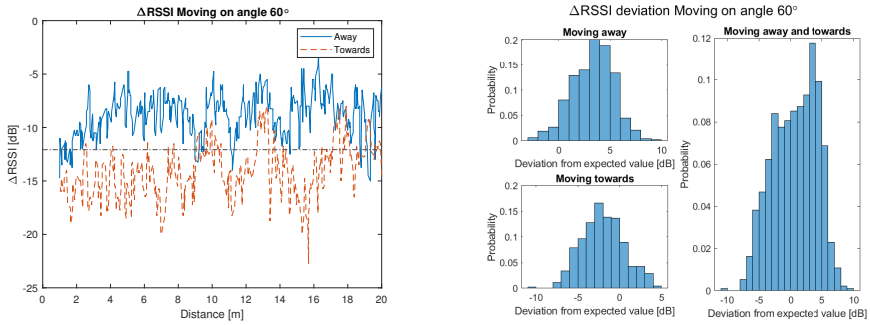

(a) Measured ΔRSSI compared with expected value

(b) Deviation of measured ΔRSSI from the expected value at the angle of interest

Figure 4.21: Movement along angle 60° on the point C

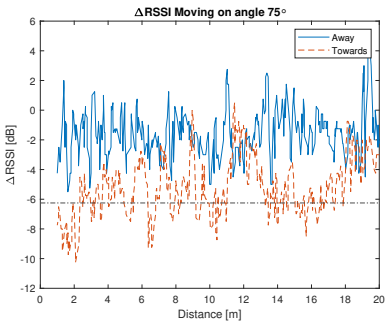

(a) Measured ΔRSSI compared with expected value

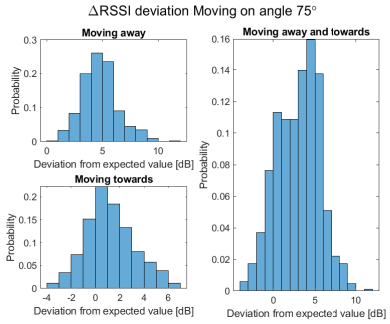

(b) Deviation of measured ΔRSSI from the expected value at the angle of interest

Figure 4.22: Movement along angle 75° on the point C

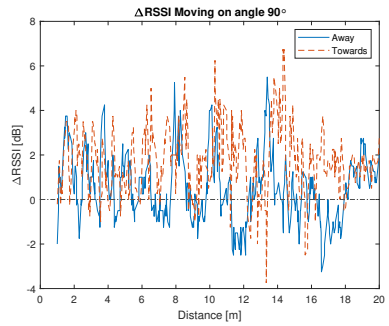

(a) Measured ΔRSSI compared with expected value

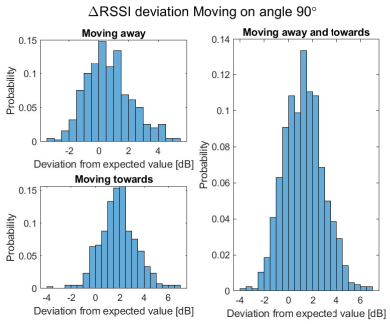

(b) Deviation of measured ΔRSSI from the expected value at the angle of interest

Figure 4.23: Movement along angle 90° on the point C

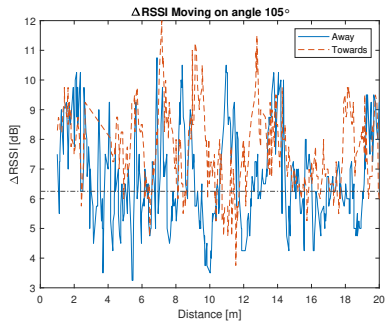

(a) Measured ΔRSSI compared with expected value

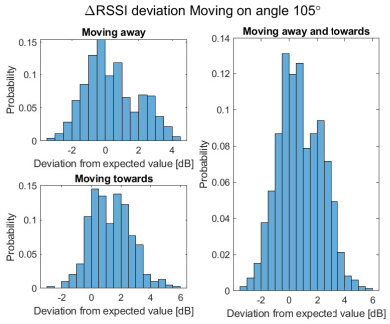

(b) Deviation of measured ΔRSSI from the expected value at the angle of interest

Figure 4.24: Movement along angle 105° on the point C

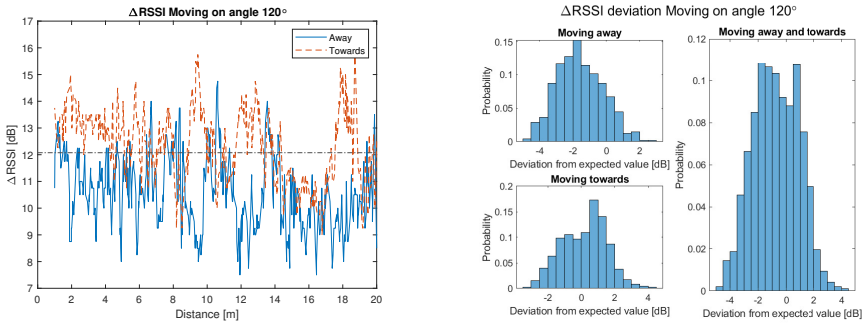

(a) Measured ΔRSSI compared with expected value

(b) Deviation of measured ΔRSSI from the expected value at the angle of interest

Figure 4.25: Movement along angle 120° on the point C

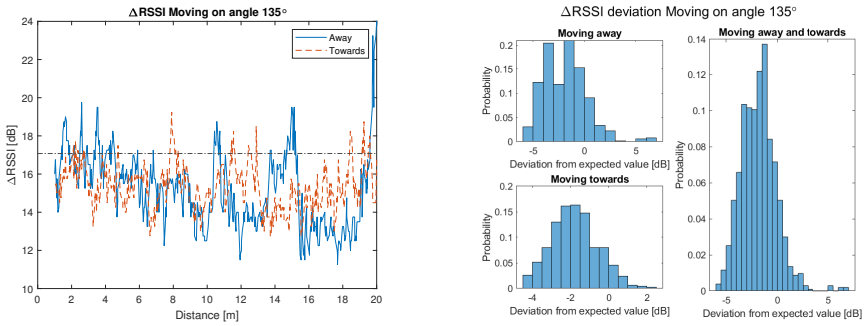

(a) Measured ΔRSSI compared with expected value

(b) Deviation of measured ΔRSSI from the expected value at the angle of interest

Figure 4.26: Movement along angle 135° on the point C

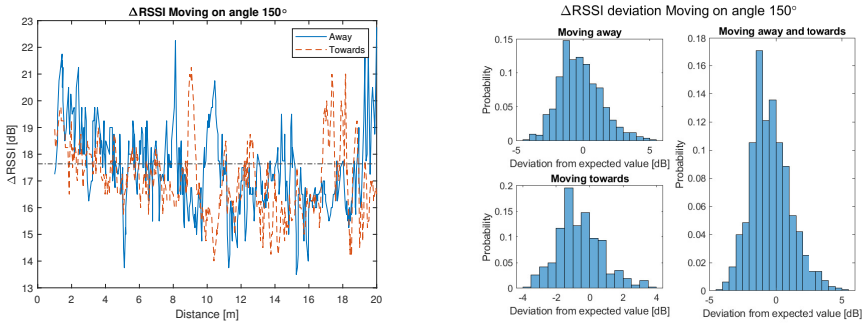

(a) Measured ΔRSSI compared with expected value

(b) Deviation of measured ΔRSSI from the expected value at the angle of interest

Figure 4.27: Movement along angle 150° on the point C

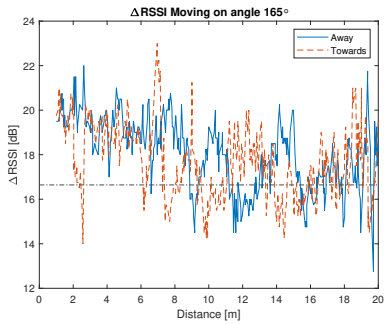

(a) Measured ΔRSSI compared with expected value

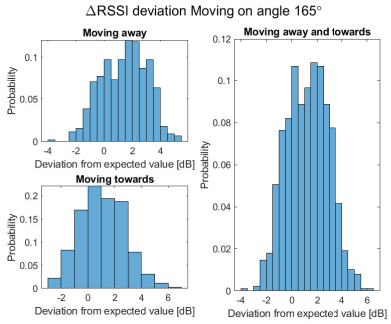

(b) Deviation of measured ΔRSSI from the expected value at the angle of interest

Figure 4.28: Movement along angle 165° on the point C

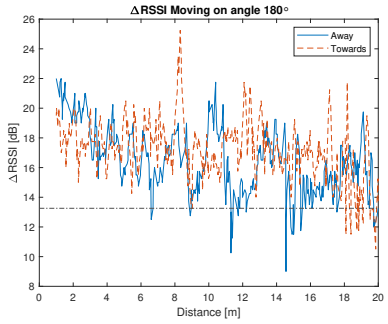

(a) Measured ΔRSSI compared with expected value

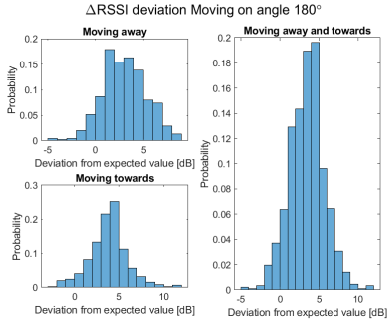

(b) Deviation of measured ΔRSSI from the expected value at the angle of interest

Figure 4.29: Movement along angle 180° on the point C

Next, we want to look at the distribution of the deviation in the measured from the expected when results from all angles are combined. Figure 4.30 displays the the distribution of the deviation of the measured ΔRSSI from its expected value at all angles of interest; this figure shows that the measured values are normally distributed around the expected value and therefore, can be modelled as a normal random variable with mean equal to 0.6 dB and standard deviation (std) equal to 2.9 dB. After analyzing the collected data, an estimation of the statistics needed to conduct the positioning field test was found to be as it follows: PLE, $\eta = 2.1$, the standard deviation of the large-scale fading, $\sigma_{LSF} = 2.1$ dB, and the standard deviation of the small-scale fading, $\sigma_{SSF} = 0.9$ dB. Statistics at each of the thirteen angles studied for this part are given in Table 4.2. Furthermore, measurement was done while moving along angle 90° for 40 m to analyze the the PLE value and to find the so-called "break-point", d_{break}, the point at which the break point used

in this analysis does not work. That point is, mathematically, given as [18]:

$$d_{break} \gtrsim \frac{4h_{TX}h_{RX}}{\lambda} \tag{4.2}$$

where, h_{TX} and h_{RX} are the heights of transmitting and receiving antennas respectively. Theoretically, d_{break} was calculated to be $\gtrsim$ 82 m. RSSI values at r_1 and r_2 of this measurement are plotted in Figure 4.31. In this measurement, it is clear that PLE value remains constant as expected from the break-point model. Furthermore, σ_{LSF} and σ_{SSF} were found to be 3.4 dB and 0.9 dB. σ_{SSF} value remains similar to the value found earlier at this particular angle, but σ_{LSF} increased by 2 dB which is the result of higher shadowing at larger distances and can be observed in Figure 4.31. This indicates a clear two path behaviour, where there is a ground reflection i.e. the received signal has two components; a LoS component and a component formed by ground reflection. Since, the height of both Transmitter (TX) and RX is low compared to higher distances covered here, the path-length distance between the LoS component and the ground reflection become very small and in turn, they are received at the same time instance; the behaviour of the received signal at the higher distance is due to destructive interference from the ground reflection component. This behaviour can be avoided by increasing the height of the antennas. The measured ΔRSSI from this measurement was also used to find $\hat{\phi}$; in Figure 4.32a, all $\hat{\phi}$ are shown, Figure 4.32b shows the distribution of error in AoA estimates. From the figure, it is clear that the error is normally distributed. The mean of the error in $\hat{\phi}$ is found to be 1° with std equal to 7°.

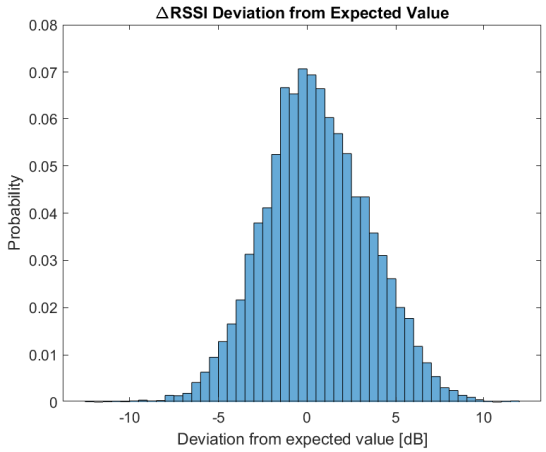

Figure 4.30: Deviation of ΔRSSI from its expected value for all angles combined.

In order to check the validity of the assumptions is chapter 2, for the relation between the $\Delta RSSI$ values and AoA, this measurement setup were used for checking the values of PLE, LSF, and SSF for each antenna. Table 4.2, shows the results for the left and right antennas. PLE values on both antennas differed with

Angle	PLE	$\sigma_{LSF}[dB]$	$\sigma_{SSF}[dB]$
0	2.1	2.2	1.0
15	2.1	2.2	1.1
30	2.0	2.0	1.2
45	1.9	2.3	1.1
60	2.1	2.5	1.0
75	2.1	2.0	0.9
90	1.9	1.5	0.8
105	2.3	1.9	0.8
120	2.0	1.5	0.7
135	2.1	2.3	0.7
150	2.1	2.3	0.8
165	2.0	2.2	0.8
180	2.0	2.5	1.0
All angles	2.1	2.1	0.9

Table 4.2: Statistics at each angle

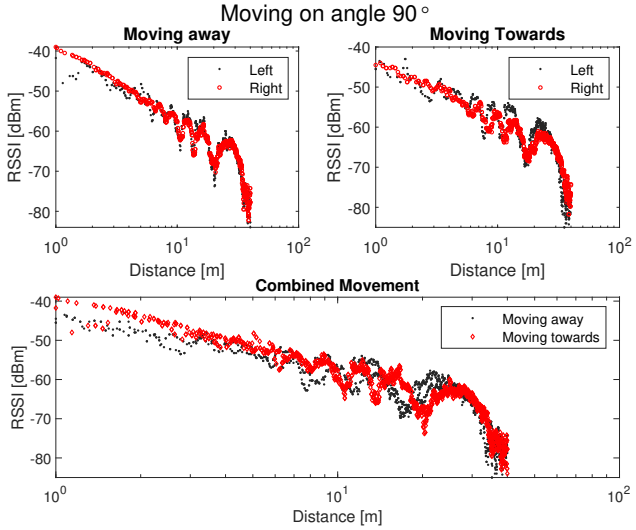

Figure 4.31: Received RSSI at r_1 and r_1.

a small value that can be ignored and can be considered the same. The values for σ_{LSF} for both antennas were close enough, that means that the LSF values on the antennas are highly correlated. σ_{SSF} values were not the same but they were close enough, but what matters for σ_{SSF} is to as small as possible. As a result, all the assumptions made in chapter 2 apply for the derived relation between $\Delta RSSI$ values and AoA. Note here that the analysis was done on raw data i.e.

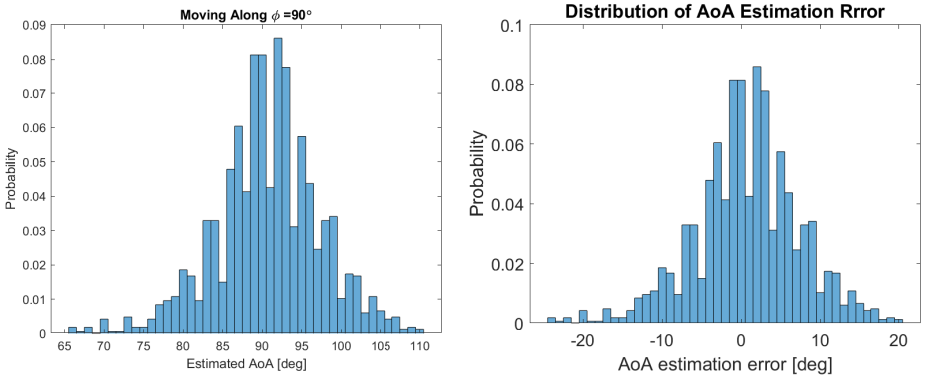

(a) Estimated AoA. **(b)** AoA estimation error.

Figure 4.32: Moving on a straight line at ϕ=90°.

no averaging was applied, so for the σ_{SSF} values after averaging the σ_{SSF} will be much more amaller, and to prove that, all the results for the AoA estimation in this chapter and the next chapter can be checked were it can be noticed that the $\Delta RSSI$ values matched the ground-truth values, and the same applies for AoA estimation.

	Left Antenna	Right Antenna
PLE	2.0	2.1
σ_{LSF}	2.2 dB	2.2 dB
σ_{SSF}	1.9 dB	1.7 dB

Table 4.3: Comparison Table for the channel statistics for the left and right antenna

4.3.3 Static Measurement

The aim of this measurement was to estimate the deviation in the AoA estimation. To do so, , TA was put still at different points at angles from 0 to 180° with an increment of 15° at the distance of 10 m and 20 m from the AP, see Figure 4.33.

A thorough analysis of the angle estimation is performed in this subsection. First, we explain issues with the estimator used to find $\hat{\phi}$. Then, the result of estimation without using averaging is shown and compared to when averaging was used. Finally, the accuracy of the estimation and a break down of the results of the linear region on the S-shape and the ambiguous region will be presented.
There are two ambiguous regions on the S-shape and it was explained in Chapter 2.3. In these two regions, our estimator will always estimate $\hat{\phi}$ that is inwards on the S-shape. As an example, in a noise free scenario, when $\phi = 0$, the estimator will give $\hat{\phi} = 60°$. In Figure 4.34, two cases are shown; (i) when ϕ=0, and (ii) when ϕ=180° in Figures 4.34a and 4.34b, respectively, where the solid black line represents the true angle at which TA was positioned. This estimation error in

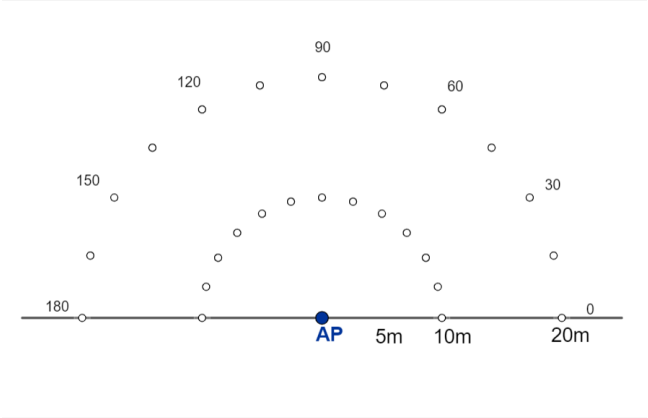

Figure 4.33: Static point at which TA was positioned.

AoA is true $\forall\ \phi\ \in [0{:}30) \cup (150{:}180]$; it must be noted that this error becomes smaller as $\phi \to \{30°\}^{-}$ or $\phi \to \{150°\}^{+}$.

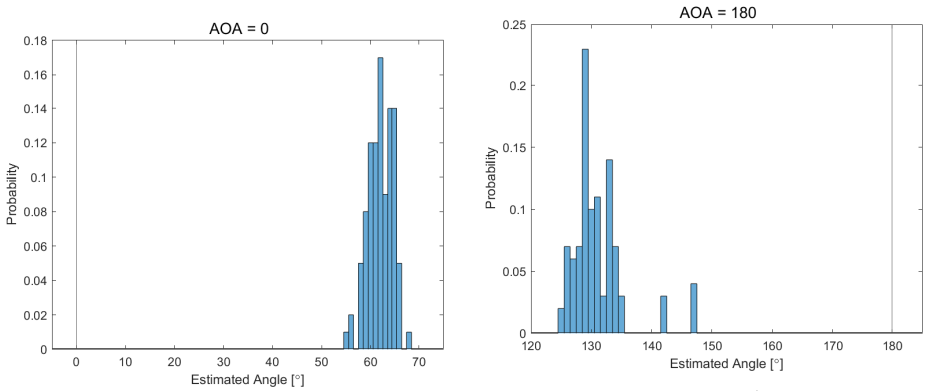

(a) Estimated AoA, $\hat{\phi}$, at true AoA, ϕ=0°. **(b)** Estimated AoA, $\hat{\phi}$, at true AoA, ϕ=180°.

Figure 4.34: Error in $\hat{\phi}$ due to look-up table usage.

Next, the effect of averaging over ten samples on AoA estimation, $\hat{\phi}$ is studied. For this, a case where TA was 20 m away from the AP at two different angles was considered. Figures 4.35a and 4.35b show two cases where TA was positioned at angles 90° and 120° on the point C. From these two figures, it can be observed that the estimation error was reduced with averaging the measured RSSI values; this reduction in estimation error is more evident in the case of 120°. Another observation is that even without averaging, the estimation was accurate up to 7 degrees. However, averaging is required to have a more accurate range estimate since range estimation depends on the received power; by averaging, range estimation can be guarded against fluctuation in received power caused by SSF.

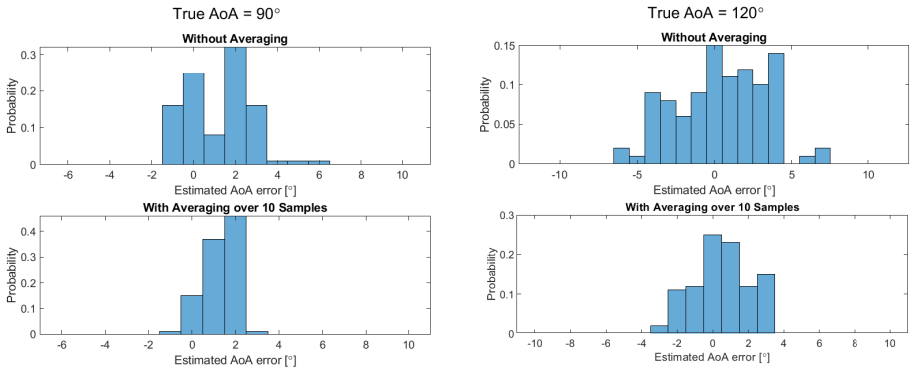

(a) Effect of Averaging over 10 samples ϕ=90°.

(b) Effect of Averaging over 10 samples ϕ=120°.

Figure 4.35: Effect of averaging on AoA estimation.

Finally, the error in measured values for all angles and distances is shown. This starts with analyzing measured ΔRSSI values which are shown in Figure 4.36. The deviation in measured ΔRSSI is normally distributed with $\sigma_{w_i} = 2.3$ dB. Comparing that to Figure 4.30, it can be observed that the two figures are similar. However, the distribution plotted here are concentrated closer to zero which makes sense since; here, the measurement were taken at static points. This makes the collected values less prone to errors caused by deviating from moving along the straight line as was the case in the previous subsection. The cause of error, here, can be contributed to inaccurate placement of TA and fluctuation in RSSI caused by SSF. Unfortunately, this distribution does not translate into a similar distribution for AoA, mainly, for shortcomings of the used estimator (look-up table). Figure 4.37a plots the distribution of AoA estimation error in which values as large as 65 degrees in error can be seen. These higher error values, however, are caused by placement of TA at angles $\Omega = \phi \in [0{:}30) \cup (150{:}180]$. To have a better view of the performance of ΔRSSI technique to estimate AoA, estimation of Ω was discarded and the resulting distribution is shown in Figure 4.37b. Here, it can be seen that majority of error in $\hat{\phi}$ lies between $\pm 10°$. σ_{m_i} in both regions of the S-shape as well as the combination of both regions are shown in Table 4.4.

Angles	σ_{m_i} [deg]
$\phi - \Omega$,	8
Ω	39
ϕ	27

Table 4.4: σ_{m_i} at different regions on the S-shape

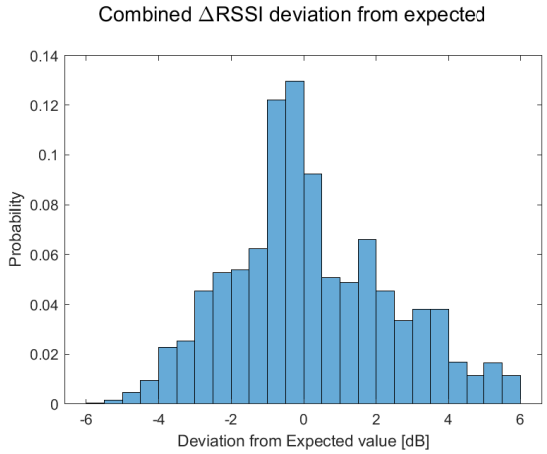

Figure 4.36: Deviation of measured ΔRSSI from the expected value.

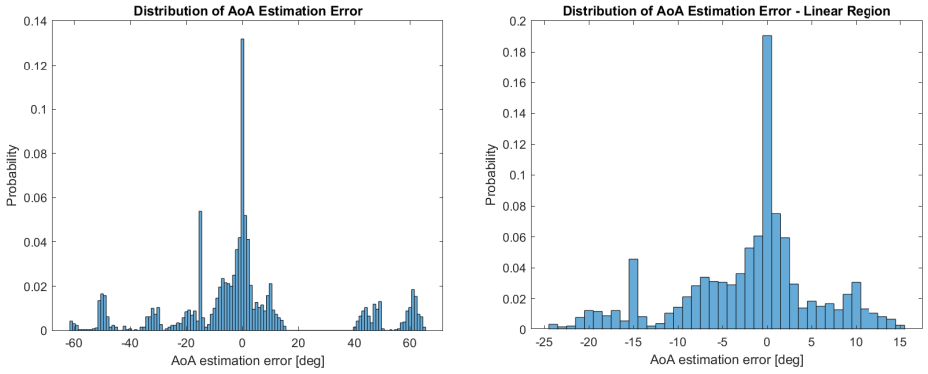

(a) Error in $\hat{\phi}$ when $\phi \in [0 \text{ to } 180°]$. **(b)** Error in $\hat{\phi}$ when $\phi \in [30° \text{ to } 150°]$.

Figure 4.37: Error in AoA estimation.

4.4 Simulations and Measurements

After the statistics of the wireless channel was obtained in the previous section, it is possible to run simulation of the localization problem using the three estimators introduced in Chapter 3. To begin, the positions of APs was defined as five point equally spaced on a circle with a radius of 20 m placed inside the square region shown in Figure 4.9. A depiction of the system can be seen in Figure 4.38a. In the next two subsections results of two simulated scenarios, one with channel statistics similar to our measurement field, and a second scenario with presence of higher noise is shown. Finally, results of field measurement is given in the last subsection of this chapter.

4.4.1 Simulation

In this subsection, a Monte-Carlo, MC, simulation was conducted to predict the performance of the proposed setup of five APs. From 4.3.3, it is known that the proposed AoA estimator is not reliable when TA is at angle $\in \Omega$ on the local x-axis of the AP. So, a simulate of the performance of the complete system i.e when all the five APs are in use is performed. For that, a trajectory was defined for the TA at 20 m away from AP_1 which is located at (20,0) on the global map as shown in Figure 4.39a and tested under two different scenarios given as: (i) a low noise scenario similar to the field measurement in the previous section with $[\sigma_{LSF} = 2.3$ dB, $\sigma_{SSF} = 0.9$ dB, $\sigma_{m_i} = 5°]$, and (ii) a high noise scenario with $[\sigma_{LSF} = 6$ dB, $\sigma_{SSF} = 4$ dB, $\sigma_{m_i} = 7°]$ with MC=1000. Figures 4.39b and 4.39c show position estimation error of scenarios (i), and (ii) respectively. The error in WLLS estimates is shown by a solid line while errors in LLS and LS estimates are shown by dashed and dotted lines, respectively. As it is evident, adding more APs did not solve the underlying problem coming from the ambiguous region i.e. when TA was at angles $\in \Omega$ on the local coordinate of one or more APs and hence, a second restriction must be put on the regions at which reliable localization is possible, heron, only estimations obtained in the white region shown in Figure 4.38c will be considered in comparing performances of the three estimators. On the other hand, when the TA was at angle $\notin \Omega$ all three algorithms in case (i) had a mean position estimation error of around 1.5 m with WLLS performing slightly better. In scenario (ii), where higher noise was present, performance of both LLS and LS estimators deteriorated considerably with a mean error of around 6.5 m; the performance of WLLS, however remained around a 2.1 m.

Next, a simulation was performed on the whole 40 m x 40 m area under same conditions in (ii) to see if the assumption of the area of reliable positioning shown in Figure 4.38c is accurate. The resulting error heat map shown in Figure 4.40 confirms the assumption about reliable localization area. From the Figure, it can concluded that the WLLS estimator outperforms LLS and LS estimators; this is evident in case where higher noise is present. Figure 4.40a displays the error heat map of the LLS estimator, Figure 4.40b displays that of the LS estimator, and finally, 4.40c displays that of the WLLS estimator.

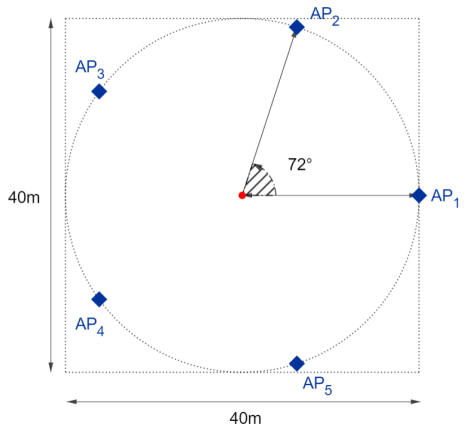

(a) System setup.

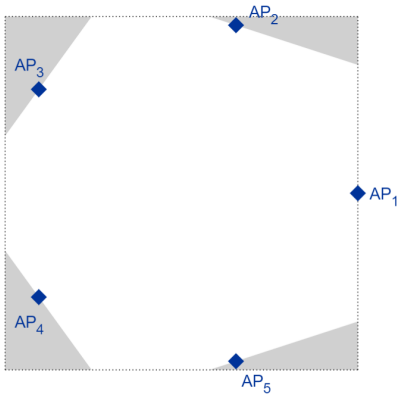

(b) LOS constraint.

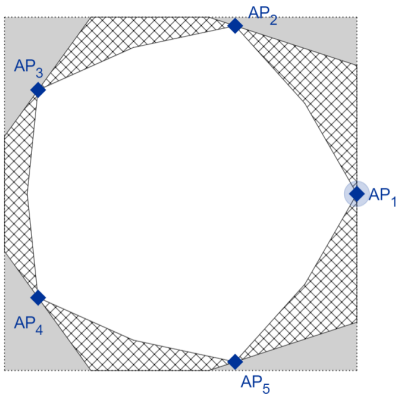

(c) Ambiguity constraint.

Figure 4.38: Setup of the system showing LOS and ambiguity constraints.

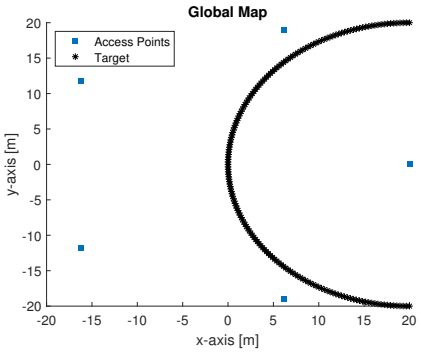

(a) Trajectory of TA on the map.

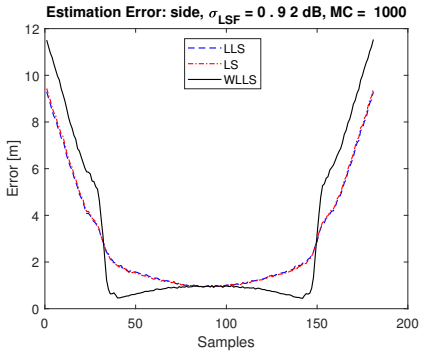

(b) Positioning error of LLS, LS, and WLLS algorithms with following conditions: $\sigma_{LSF} = 2.3dB$, $\sigma_{SSF} = 0.9dB$, and $\sigma_{w_i} = 5°$.

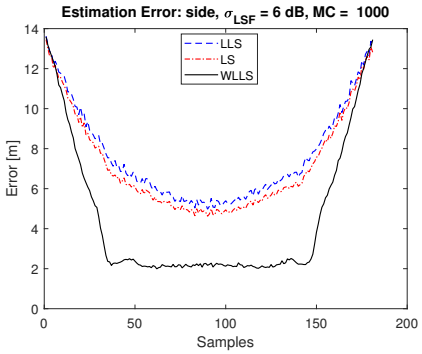

(c) Positioning error of LLS, LS, and WLLS algorithms with following conditions: $\sigma_{LSF} = 6dB$, $\sigma_{SSF} = 4dB$, and $\sigma_{w_i} = 7°$.

Figure 4.39: Simulation results of two noise level scenarios.

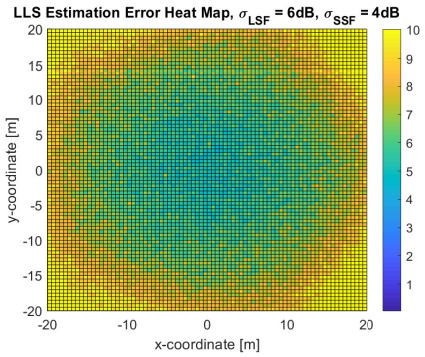

(a) LLS algorithm.

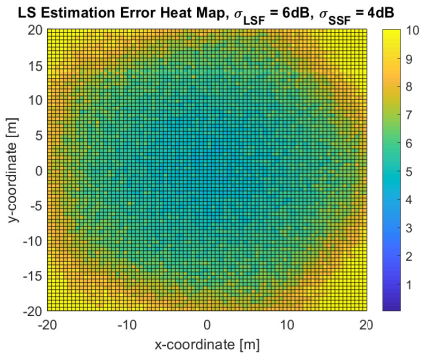

(b) LS algorithm.

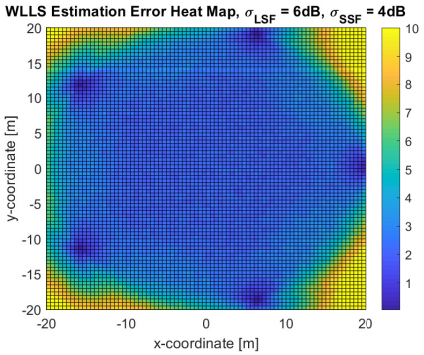

(c) WLLS algorithm.

Figure 4.40: Performance of localization algorithms under the following conditions: σ_{LSF} = 6 dB, σ_{SSF} = 4 dB, σ_{ν_i} = 7°.

4.4.2 Field Measurement

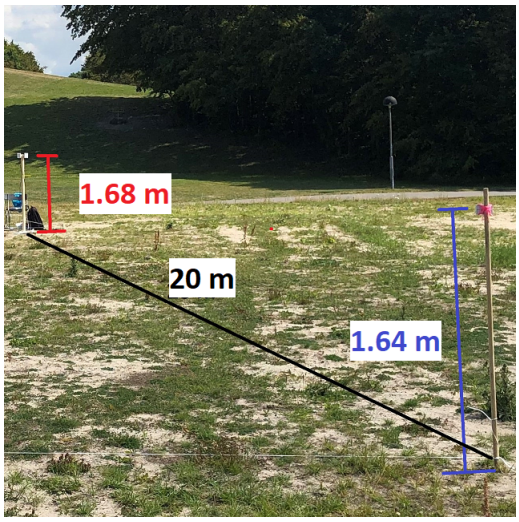

Figure 4.41: Measurement equipment.

The next part of the thesis is to conduct a field test and apply the algorithms to compare the practical results to results obtained from the simulation in 4.4.1. The original plan was to test the system using five APs with a moving TA and perform real-time positioning. Unfortunately, the facilities needed for this experiment was not ready by the time the field test was supposed to be performed. Hence, with only one AP available, a virtual measurement was performed with static points. For the experiment, 45 points were selected on the field as shown in 4.42a, where the filled circles represents those in the good region and the others represent those in the ambiguous region of AP_1. Measurements were done at all points for one AP and then the AP setup was moved to the position of the next AP and so on. Figure 4.42b shows the mean error over ten position estimations using the three estimators; this plot is divided in two regions by a dashed vertical line. As evident WLLS performance is more accurate than the other two estimators. The mean error of the estimation is shown in Table 4.5. Finally, position estimates using WLLS estimator is shown in Figure 4.43.

Region	WLLS	LS	LLS
Linear region	2.06 m	4.15 m	4.48 m
Ambiguous region	5.72 m	16.82 m	19.35 m
Overall	3.19 m	8.09 m	9.11 m

Table 4.5: Mean error in position estimation in all estimators

These results found here have the potential to be improved considerably given that this measurement was conducted virtually which opens the door to several

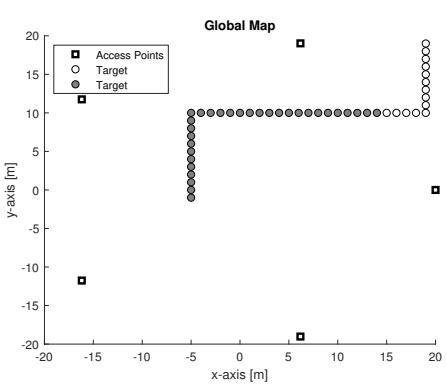

(a) Target positions on the field.

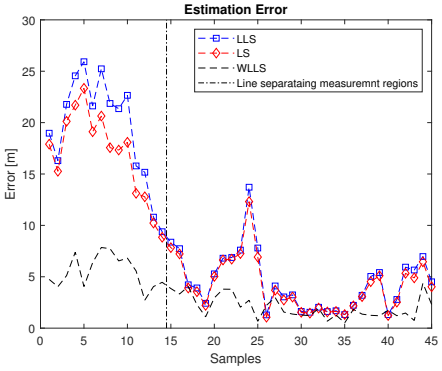

(b) Error in position estimation of the three estimators.

Figure 4.42: Measurement results.

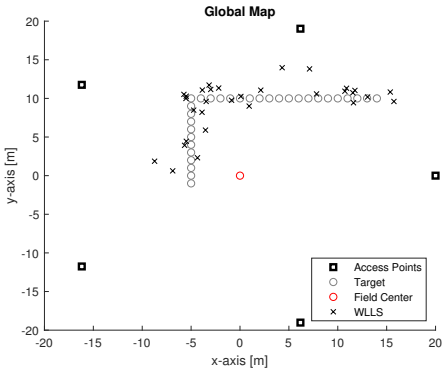

(a) Estimated position using WLLS estimator in the good region.

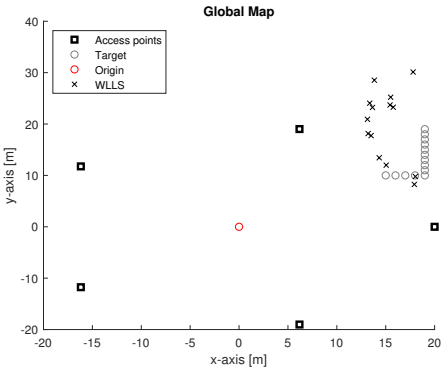

(b) Estimated position using WLLS estimator in the ambiguous region.

Figure 4.43: Estimated positions using WLLS.

measurement errors. For instance, taking measurements at each point for different AP's meant that TA was moved every time the measurements of one AP was finished. any misplacement of the TA affects the result of the positioning. Secondly, it was mentioned in section4.2.1 that the pattern of the TX was not omni-directional and that the received power was very sensitive to the orientation of the TX. Hence, it was essential to maintain the orientation of the TX relative to the antennas at the AP. This however opens the door for a bigger problem; that is the orientation of TX is different relative to each A. hence, it is recommended to conduct the measurement using a TX that perfectly omni-directional.

4.4.3 Non-Line of Sight AoA Estimation

Until now, only LoS situations were considered. in this short subsection, we will briefly look into a NLoS situation where there is no clear path between TX and RX. Here, two cases are considered: (i) static points in cases where there is no clear path between TX and RX due to terrain or vegetation, (ii) movement along an arc in the same environment in (i).

Static Measurement in a NLoS scenario

For this measurement, two point as shown in Figure 4.45 are chosen; one is located 37 m away at angle 90° on the local axis of the AP, located behind a hill. The second point is located 36.44 m away on the angle 164° on the local axis of AP and was placed behind a group of trees. The mean and standard deviation of the error in AoA these cases are given in Table 4.6

Scenario	μ_{Error}	σ_{Error}
Terrain	14°	3°
Vegetation	16°	3°

Table 4.6: Mean and standard deviation of the error in AoA estimation

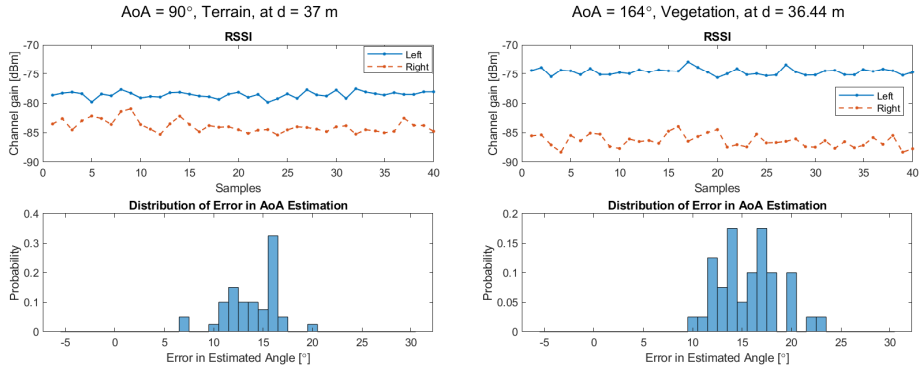

(a) Obstruction by terrain. **(b)** Obstruction by vegetation.

Figure 4.44: NLoS scenario: Received power at r_1 and r_2 (top), Distribution of Error in AoA estimation.

Movement in a NLoS Situation

For this subsection, data was collected while the TA was moving on an arc-like trajectory, See Figure 4.45. Here, direct path between TX and RX was obstructed by a combination of vegetation and terrain. In order to get the ground-truth angles, it was assumed that the TA was moving at a constant speed of 1 m/sec

so that the position of TA at the time of transmission could be estimated; this translates into a bias in the ground-truth angles that are used for comparison and estimation of error in AoA. In Figure 4.47a received power at r_1, and r_2 is shown and the resulted ΔRSSI is plotted against its theoretical expected value according to what was estimated to be the ground-truth angle of TA's position in Figure 4.46. It can be seen that the measured values follow closely the theoretical S-shape, albeit, with higher fluctuations compared to what was found in chapter 4.3.1. These higher fluctuations will indeed result in higher inaccuracies in the estimation of AoA which is shown in Figure 4.46. In this figure, estimated AoA is plotted as a dashed-line against the ground-truth angles. To avoid confusion, it should be noted that movement starts at angle 180° and ends at angle 90°. Finally, the mean of error in AoA estimation was found to be 15° with a standard deviation of 20°. The results found here are acceptable for a NLoS situation. It is of high importance to mention that the ground-truth angles to which the estimations were compared were estimates based on an assumption of constant speed and movement along an arc. This in reality, could not be the true angles and hence will add a bias to the AoA estimation errors. In the considered movement, two angles are certain to be true angles and those are the angles at the start and the end of the movement; looking closely at Figure 4.47b, it can be seen that, indeed, ΔRSSI at the start and end of the measurement lie on or very close to the theoretical curve; while other points follow the theoretical curve closely but with a shift to the right. In such a scenario, the estimation error would be much lower than what is stated above. Unfortunately, it was not possible to gain the ground-truth information about the path of TA due to natural obstacles.

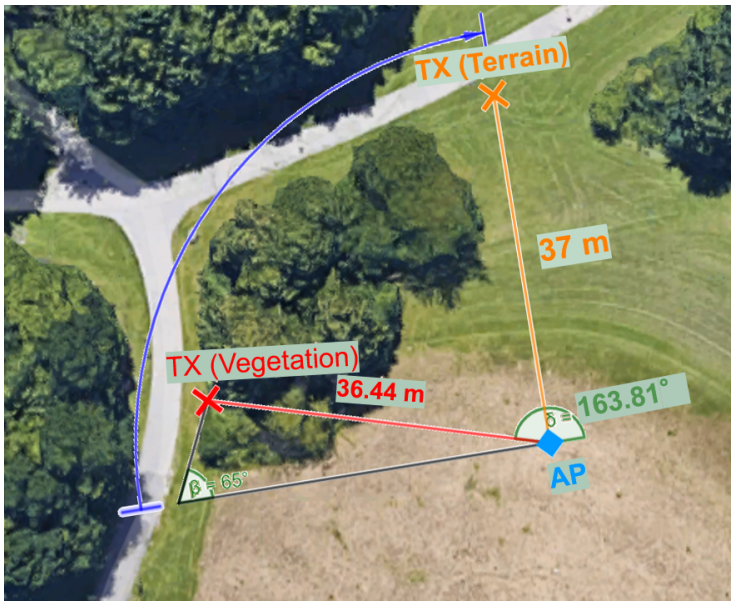

Figure 4.45: Bird's eye view of NLoS measurement location.

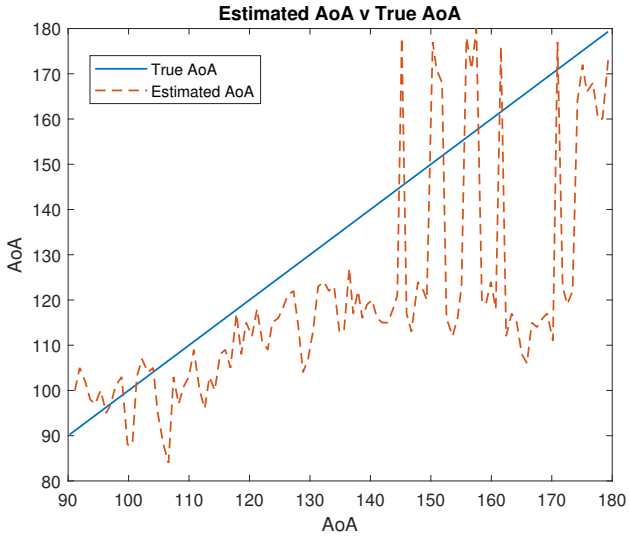

Figure 4.46: NLoS AoA estimation.

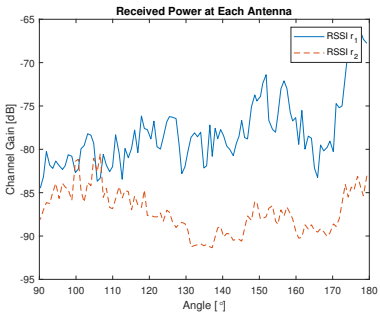

(a) Power received at AP.

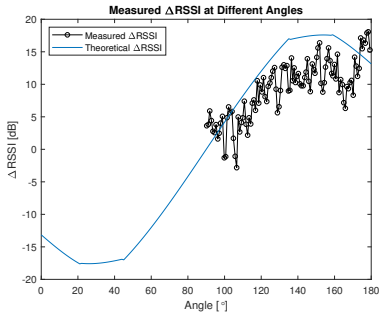

(b) NLoS measured ΔRSSI.

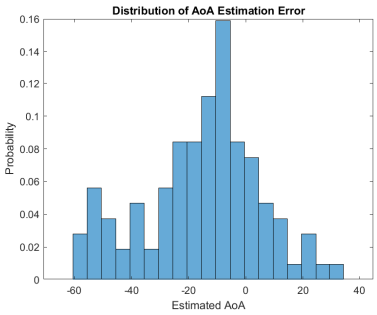

(c) Distribution of error in AoA estimation, moving TA.

Figure 4.47: NLoS movement field measurement results.

Chapter 5

LoRa System

5.1 LoRa Overview

In the previous chapter, a BLE system equipped with a dual antenna setup was discussed, and it is known that BLE systems can have reliable communication link up to 100 meters in a line of sight environments, and up to 50 meters in non-line of sight environments. So for these ranges are enough to have a dual antenna setup at each access point with a WLLS positioning estimator, as it gave the expected results for the outdoor measurement as it was explained in chapter 3. So what it is required to estimate the position or AoA for longer ranges? Is it enough to have the dual antenna setup for the AoA estimation? What happens for the position/AoA in a more complicated environments such as estimating the position of a target moving inside the city? The answers for these questions are discussed in this chapter.
Here, LoRa technology will be used instead of BLE technology, the 4-antenna setup that was discussed in chapter 2 and the corresponding AoA sector estimator is used instead of the dual antenna setup. So why LoRa technology and the four antenna setup were chosen for the aimed goal?
Simply, as Multiple Input Multiple Output (MIMO) and IoT systems are one of hot the topics in the communications field nowadays, and for it is expected that thousands of nodes and sensors will be deployed in the coming years. Localization solutions other than GPS are a necessity, since GPS modules are expensive compared to the prices of the deployed nodes, and these GPS modules consumes a lot of power. An efficient solution is considered, which is the LoRa technology, as it is one of the most power efficient technologies available in the market; the prices for the LoRa modules are cheaper compared with other communication technologies modules and LoRa can achieve reliable long range communication links, but with trade of small bandwidth and low data rates.
For the localization solution that is considered, the four antenna setup will be tested in different environments, and will show that the angular accuracy crossed the expectations using the simple AoA sectors estimator that is explained in chapter 2. Two APs will be used to estimate the position of a TA, and it is noticed here that the number of APs used for the LoRa system is less than that of the BLE systems. That is because higher AoA accuracy was achieved which will compensate for the less number of APs.

5.2 Hardware

LoRa is a wireless modulation optimized for power efficient long range communication link which uses Chirp Spread Spectrum (CSS) modulation [12]. CSS is a power efficient modulation that achieves low power constraints and achieves longer ranges than other low power modulation like Frequency Shift Keying (FSK). LoRa is the first low cost implementation of CSS for commercial usage. Long range capability is the advantage of LoRa, as single gateway can handle thousands of deployed nodes and can have coverage in the kilometers range. The most critical factors of Low-Power Wide-Area Network (LPWAN) are: communication range, long battery life time, network architecture, diversity of applications served, interference immunity, network security, and network capacity.

Communication range:

Technology	Wireless Communication	Range
Bluetooth	Short range	10 m
WiFi	Short range	50 m
3G/4G	Cellular	5 km
LoRa	LPWAN	• 2-5 km (urban) • 5-15 km (rural) • >15 km (LoS)

Table 5.1: Range of different communication technologies

Long Battery lifetime:

The nodes in a Long Range Wide Area Network (LoRaWAN) are asynchronous, and whenever a data is ready to send these nodes start the communication. That saves a lot of power that make the batteries last for longer time [13].

Network architecture:

LoRaWAN uses long range star architecture that preserves battery lifetime while achieving long-range connectivity [13].

Diversity of applications served:

Applications include asset tracking, monitoring, cold chain monitoring, equipment tracking, leak detection, logistics and transportation management, parking space monitoring, environmental monitoring, temperature monitoring, waste bin monitoring, and much more [14].

Interference immunity:

1. Co-channel interference: This happens when some other transmitters use the same frequency which the device is using. If interference is 10 dB weaker than

the received signal, many RF systems stop functioning. With LoRa, the receiver will still be functioning even when the interference is as much as 19 dB larger than the received signal. This means that for crowded frequency channels LoRa systems will keep working reliably.
2. Blocking Rejection: in the existence of a powerful interfering signal near the operating LoRa device, even though LoRa is 10 times more sensitive, it is even 20 times less vulnerable to overload from powerful out-of-band signals [15].

Network security:

LoRaWAN uses two layers of security: the first one is for the network and the second one is for the application. The network security ensures the authenticity of the node in the network, while the application layer ensures that the network operator cannot access end user's application data [16].

Network capacity:

LoRaWAN achieves high network capacity by using adaptive data rate by choosing different spreading factors and by using a multi-channel transceiver in the gateway so that the gateway can receive simultaneous messages from multiple channels[13]. LoRa regulations in Europe is shown in Table 5.2 [17].

	Europe
Frequency Band	867-868 MHz
Channels	10
Channels BW DL	125/250 kHz
Channels BW UL	125 kHz
Tx Power	14 dBm
SF	7-12
Data Rate	250 bps - 50 kbps

Table 5.2: LoRa regulations in Europe [17]

In order to test the proposed AoA sector estimator, a LoRa receiver system is designed. The system consists of eight LoRa modules that will act as receivers, eight directive antennas operating in the 868 MHz, a field test device that will act as the transmitter, and two antenna holders. Figure 5.1 shows the antenna radiation pattern in the horizontal and vertical plan, and Table 5.1 shows the electrical and the mechanical specifications of the antenna [28]. It can be noticed from Table 5.1, that the size of the antenna is large, since the antenna size is proportional to the wavelength, and the operating frequency range of this antenna is in the $\sim$868 MHz, so the corresponding wavelength is $\sim$35 [cm]. For the four antenna setup and to place antennas of such size at 45° separation angle, a special holder was designed, the material for the designed holder was wood, that has minor affect on the radiation pattern of the antenna, as it can be seen in Figure 5.2.
Another important parameter from Table 5.1 is that the beam-width of the radi-

(a) Horizontal Beam-Width 60°. **(b)** Vertical Beam-Width 55°.

Figure 5.1: Antenna Radiation Pattern.

Electrical Specifications	
Model	CF-RA9002
Frequency Range MHz	865∼868
Gain	9 dBi
Horizontal Beam-Width	60
Vertical Beam-Width	55
Polarization	Circular
Mechanical Specifications	
Siza (mm)	257x267x33
Antenna Weight (Kg)	1

Table 5.3: LoRa antenna specifications

ation pattern is 60°, so it complies with synthetic radiation that was generated in Chapter 2. The maximum gain of the radiation pattern of the antenna is 9 dBi, so the synthetic radiation pattern was modified in order to comply with this gain value. The side lobes and main lobe of the actual radiation pattern were close enough to synthetic radiation pattern, but still there will be some minor effects on the lookup table but for now these effects were ignored as it was a proof of concept project, and in case that the proposed estimator to be used in a real time application, it is preferred to measure the actual radiation pattern in the anechoic chamber. For the LoRa modules, "TTGO LORA32 915MHz ESP32 LoRa Development Board Module With Antenna" in Figure 5.3 was used during this project, as the price of these modules were within the budget of this project. The module has an on board UFL connector, that it provides flexibility to the choices of the antenna, the board contains a wifi antenna that made it easier for the authors while doing the experiment to connect all the modules to a centralized place for logging the data, without the need for more complicated solutions, the receiver sensitivity is about -148 dBm, operating voltage: 3.3 V to 7 V with a micro-USB connector, that can be powered by a power bank which make life easier when comes to outdoor measurements, and it supports Arduino development environment.

The LoRa modules were programmed using [29] 1-channel gateway that is cre-

Figure 5.2: Antenna Holder and Four Antenna Setup.

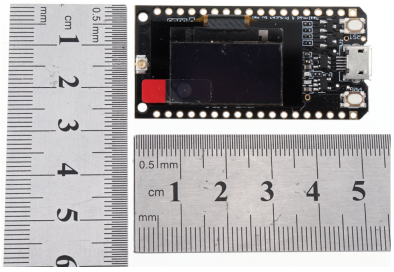

(a) Horizontal Beam-Width 60°.

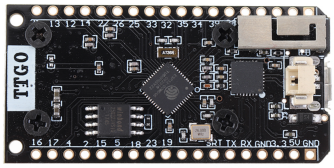

(b) Vertical Beam-Width 55°.

Figure 5.3: Antenna Radiation Pattern.

ated by "M. Westenberg" and it is an open source and it is license free. The authors modified many parameters in this code that make it compliant with the frequency regulations in Sweden, working on this specific LoRa module, and many other configuration settings. The LoRa module was programmed to act like any LoRa gateway but the authors opted not register the gateway to the The Things Networks, so it can work as a sniffing tool. The authors tried to make the single channel gateway to be working on all the available frequency channels but there was an unexpected behaviour that even the owner of the code could not solve. So as the LoRa module will be listening on only one channel this made life harder when it comes to the time spend on the outdoor measurements as the transmitter was using a pseudo-random frequency hopping, and some unexpected performance when it came to the positioning in the city, as will explained later in this chapter.

The transmitter was an "Adeunis Field Test Device" [30], that is a ready-to-

Figure 5.4: Adeunis Field Test Device.

use LoRa field test device, with range up to 15 km, high precision GPS, and self-powered and rechargeable. It operates in two modes, the first mode is an advertiser that continuously transmit packets that contains it position, while the second mode is a two way communication where it connects to nearest LoRaWAN gateway. When the field test device operate in the second mode there is no control over the frequency hopping pseudo-random sequence as it is controlled by the LoRaWAN gateway. The transmitted packet is encrypted using a network security key and an application security key that are provided by The Things Network, and these keys were determined in the initializing phase, and each time the device is turned on these keys and the device address were changing, so it is recommended that each time this device is used to record these keys because they are critical when it comes to the decryption process.

5.3 Experiments Setup and Results

In order to evaluate the AoA sectors estimator in a real time environment, three experiments were performed. The first experiment was to check the accuracy of the estimated AoA and get some channel statistics, the second experiment was to determine the position of the field test device in a line of sight short range environment using two access points each access point equipped with four antennas, and the third experiment was to determine the position of the field test device in the city of Lund for longer range and a complicated environment.

5.3.1 AoA Estimation in LoS Environment

Chapter 4 showed that the accuracy of the estimated AoA is good in the linear region from 60° to 120° while, the estimation was bad in the ambiguity regions, and as it was mentioned in Chapter 2, that the four antenna setup combined with the AoA sectors estimator will result in a higher accuracy of the AoA. So in order to test the four antenna setup and the AoA sectors estimator, an experiment was executed in the archery field at "Sankt Hans backar, Lund". The access point position in the field and the direction of antenna can be shown in Figure 5.5, where at each of the specified angle the target was moving from 20 meters range toward the access point with constant speed. The ground truth range and angle of the target were measured precisely, since the ground truth values are important for the comparison between the estimated AoA and measured angle of the target's position.

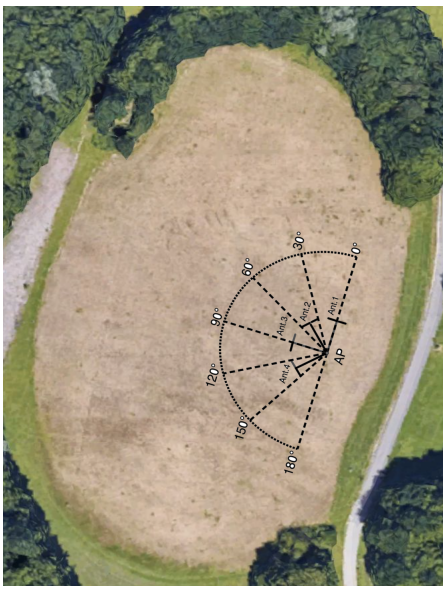

Figure 5.5: Experiment 1 Place and Setup.

The field test device operated in the advertiser mode, that will use three frequency channels 868.1 MHz, 868.3 MHz, and 868.5 MHz. The receivers was tuned to the 868.1 MHz frequency channel. For the transmitter to send a packet at 868.1 MHz was totally a random process. The velocity of the target was so slow in the range of 8 cm/sec and the total number of packets was at most 20 packets for the 19 meters movement toward the access point, which took almost 30 min for each movement along a straight line at specific angle. The aim for this experiment is to have as much as possible packets in order to estimate the statistics of the channel such as PLE, LSF, and SSF. However, the total number of received packet were 88 packets for all the movements, that make the authors excluding the statistical study for this experiment.
The result of the AoA estimation errors are shown in Figure 5.6, where the mean

value was around -1°, and the standard deviation was around 8°. Considering the whole range of angles from 0° to 180°, this is a huge improvement compared to the same experiment using the dual antenna setup in Chapter 3. It is important here to note that the results shown in Figure 5.6 are for the raw data, because averaging was not applicable, since the number of samples were so low, and in case that the frequency hopping issue is fixed at the receiver and there will be no lost packets because of the limitations in the receiver this result can improve much more, specially for the standard deviation that will be more narrow.

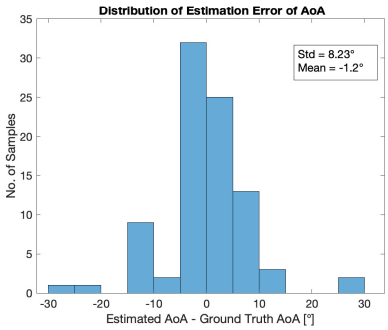

Figure 5.6: Angular Error Distribution.

In order to investigate the channel effect on the received $\Delta RSSI$ values, the difference between the measured $\Delta RSSI$ and the mean value of $\Delta RSSI$ is in Figure 5.7. The mean of this difference was 0 dBm, and the standard deviation was around 1.7 dBm, which means that with out averaging and for 19 meters distance of movement for the target, the variations in the channel where acceptable. Depending on these results, the AoA sectors estimator was functioning as expected

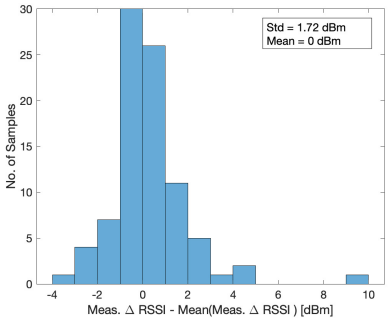

Figure 5.7: [$\Delta RSSI$ Error Distribution.

and it can be used in a localization system as in the next experiment.

5.3.2 Localization at an Open Field

In order to evaluate the accuracy of the target position, and depending on the resolution of the estimated AoA, a test in the field of "Sankt Hans backar, Lund" was conducted, two access points were used and each access point was equipped with a four-antenna setup as it can be seen in Figure 5.8; the target was located in positions as shown in Figure 5.8. The transmitter were operating in the advertiser mode, and the receiver were tuned to the 868.1 MHz. The LS position estimator were used to determine the location of the target, as the weighting is done on the ranges, and the range was estimated using the Law of Sines in a triangle formed by the two estimated ranges and the distance between the two access points, the angles inside the triangle were the two estimated AoA. Using the Law of Sine the relation between the estimated AoA and the range estimates is a proportional relation, so using the LS position estimator that gives the weights for the APs based on the range estimates is equivalent to give the weights based on the estimated AoAs. Figure 5.9(b), shows the actual target's positions and the estimated positions, and

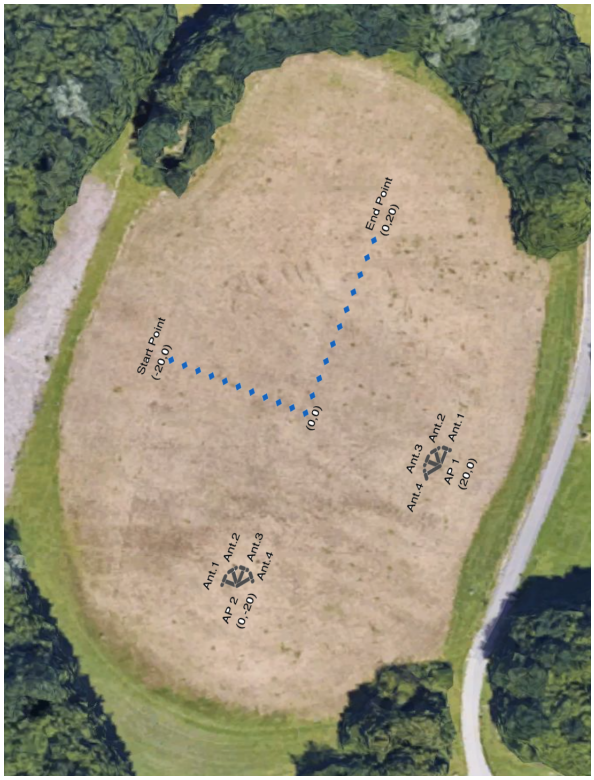

Figure 5.8: Measurement 2 AP positions and movement.

as it can be seen that the estimations were almost correct except for the first 5 points. Figure 5.9 (b) shows the error in the position, and the mean of error was 3.4 meters and the standard deviation of the error was around 3.2 meters. The expectations of the error for this experiment was around 10 meters, and the

estimated positions passed the expectations. Still, for the first 5 points there was a high error in the estimated AoA as it can be seen in figure 5.10, and that was because for these points the antennas 1 and 2 received less power than the expected so it affected the AoA estimation that resulted in an error of the position estimations. LS estimator should give less weight to the AP having more error in the AoA than the other, but using just two access points the position estimators will suffer from these kind of behaviours. So it is recommended to use three access points instead, that will improve the results.

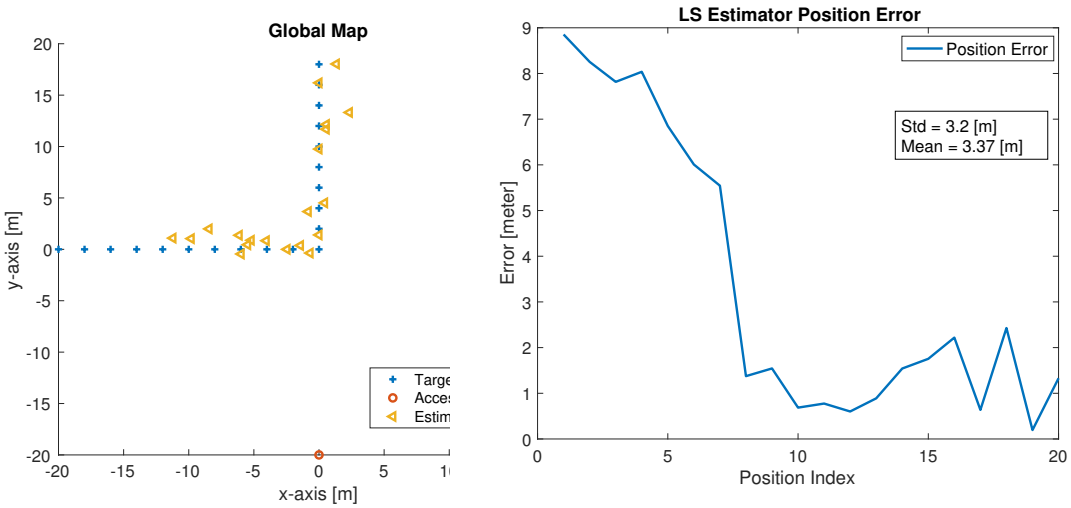

(a) Estimated Positions Error.

(b) Actual Positions vs. Estimated Positions.

Figure 5.9: Experiment 2 Results.

5.3.3 AoA City Measurement

The final experiment was to deploy the two access points that are equipped with the four antenna setup at two hills in Lund city, as the positions of the two access points and the target movement within the drawn circle are shown in Figure 5.10. The transmitter operated in the two way communication in order to have the ground truth positions of the target logged in the TTN. The receiver was tuned to the 868.1 MHz at the start of the experiment then it was tuned to the 868.3 MHz. The experiment however failed as there was no reliable connection between the target and the two access points. Unfortunately, due to time constrains this measurement is left for the future work. For the city experiment to have acceptable results, the reception issue should be solved, so that the receiver should be able to receive all/most the packet at all frequency channels and all the spreading factors.

Figure 5.10: Measurement 2 AP positions and movement.

Chapter 6
Conclusions

Developing a new technique for estimating the AoA from the RSSI difference, was a challenging task and of vital importance. Since RSSI values are sensitive to the channel/propagation conditions and to show that the RSSI difference is immune to the channel/propagation conditions using two sensitive RSSI values, demanded extensive study and many measurements in different channel/propagation conditions in order to check the validity of the proposed technique. The requirements for the AoA estimation were met, and the device friendly requirement were achieved by having two external antennas and a receiver capable of receiving simultaneous RSSI value from the external antennas. The simplicity requirement were achieved by using hard decision estimation, so that the only operation required from the receiver is to calculate the difference between simultaneous RSSI values from the antennas and to extract the AoA value from a pre-logged look-up table for this RSSI difference value. So, the other requirement needed from the receiver is to have enough memory space for the look-up table. Many measurements took place in order to evaluate the accuracy of estimated AoA, and to check the validity of the assumptions for the AoA from RSSI difference. The results complied with expectations. As the accuracy of the AoA was 8° which is better than the 10° expected AoA accuracy. In many cases and under different channel/propagation conditions the AoA matched the ground-truth angles of the target's position that indicates that the assumptions that were taken for the AoA from RSSI difference were valid. For the positioning measurement in BLE, using the virtual setup affected the position estimation accuracy, but still the results were acceptable as the position accuracy was 2 m for the linear region and around 6 m for the ambiguous region. So, with five access points these results are expected to comply with the expectations of less than a meter position accuracy. This opens the door for new range estimation techniques that are not dependent on the AoA estimates or RSSI values that will enhance the positioning result furthermore. For the NLoS scenarios, the angular accuracy achieved was around 15° that is better than that of the expected 20° for the same scenarios. In the LoRa section, the four antenna setup and the AoA sector estimator improved the accuracy of AoA and extended the range of angles that can be trusted for the estimated AoA. The positioning measurement proved that the position accuracy was 3.5 m which is less than the 10 m expected position accuracy. The LoRa city measurement failure, was not expected, and drives new challenges for the authors to improve the system to the level that can achieve the expected position estimate in the city.

Finally, it is worth emphasizing that the main goal of this thesis work is achieved and the objectives are met. The details about increasing the AoA estimates accuracy and achieve the position accuracy are provided in future work chapter.

Chapter 7
Future Work

In this section, several important aspects are highlighted to be considered for the future work and development.

- A real-time BLE localization measurement with all five access points online in order to have a true evaluation of the accuracy of the AoA and position estimates.
- Remove the range estimation dependency from the AoA estimates since inaccurate AoA estimate will result in wrong range estimate for the RSSI model used in this thesis work.
- Improve the AoA accuracy using more advanced estimation theory techniques, as this thesis work showed that the concept of ΔRSSI-based AoA estimate is valid and the next step is to get more out of this estimation technique in order to reach the highest possible accuracy.
- Test the positioning for LoRa using one access point equipped with the eight-antennas setup to estimate the position of a moving target, since this thesis work has showed that there exists a possibility for such.
- Repeat the LoRa city measurement and get the suitable configuration for the system and examine the AoA accuracy in a complicated environment such as the city.

References

[1] The European Telecommunications Standards Institute, *5G*, `https://www.etsi.org/technologies/5g`. Fetched on 15 June 2019.

[2] Nordigi AS, *Prediction and Expectation of IoT*, `https://nordigi.no/index.php/en/blog/57-prediction-and-expectation-of-iot`. Fetched on 10 June 2019.

[3] Z. T. Al-Azez, A. Q. Lawey, T. E. H. El-Gorashi and J. M. H. Elmirghani, *Virtualization framework for energy efficient IoT networks*, 2015 IEEE 4th International Conference on Cloud Networking (CloudNet), Niagara Falls, ON, 2015, pp. 74-77. doi: 10.1109/CloudNet.2015.7335284

[4] R. M. Buehrer, S. Zekavat, *Handbook of Position Location: Theory, Practice, and Advances*, 2nd ed.; John Wiley and Sons, Inc., Hoboken, New Jersey, USA, 2019

[5] ScienceDirect, *Received Signal Strength*, `https://www.sciencedirect.com/topics/computer-science/received-signal-strength`. Fetched on 1 August 2019.

[6] S. Tomic, M. Beko, R. Dinis, L. Bernardo, (2018). *On Target Localization Using Combined RSS and AoA Measurements*. Sensors. 18. 1266. 10.3390/s18041266

[7] J. Jiang, C. Lin, F. Lin and S. Huang, *ALRD: AoA localization with RSSI differences of directional antennas for wireless sensor networks*, International Conference on Information Society (i-Society 2012), London, 2012, pp. 304-309

[8] R. Javaid, R. Qureshi, R. Enam. (2015). *RSSI based Node Localization using Trilateration in Wireless Sensor Network*. Bahria University Journal of Information & Communication Technologies. 8. 58-64

[9] D. E. Manolakis, *Efficient solution and performance analysis of 3-D position estimation by trilateration*, in IEEE Transactions on Aerospace and Electronic Systems, vol. 32, no. 4, pp. 1239-1248, Oct. 1996.

[10] A. H. Sayed, A. Tarighat, N. Khajehnouri, *Network-based wireless location: challenges faced in developing techniques for accurate wireless location information*, in IEEE Signal Processing Magazine, vol. 22, no. 4, pp. 24-40, July 2005.

[11] Bluetooth SIG. `https://www.bluetooth.com/about-us/our-history/`. Fetched on 1 July 2019.

[12] B. Reynders and S. Pollin, *Chirp spread spectrum as a modulation technique for long range communication*, 2016 Symposium on Communications and Vehicular Technologies (SCVT), Mons, 2016, pp. 1-5. doi: 10.1109/SCVT.2016.7797659

[13] A. Augustin, J. Yi, T. Clausen, W. Townsley, (2016). *A Study of LoRa: Long Range & Low Power Networks for the Internet of Things*. Sensors. 16. 1466. 10.3390/s16091466

[14] J.Blackman, *What IoT applications does LoRaWAN serve best?*, 2019 `https://enterpriseiotinsights.com/20190722/channels/fundamentals/what-iot-apps-are-best-with-lorawan`. Fetched on 15 July 2019

[15] J. Sonnenberg, *The LoRa Protocol*. Raveon. (2015) `https://www.raveon.com/wp-content/uploads/2019/02/AN205LoRa.pdf`. Fetched on 21 August 2019.

[16] Smart Makers, *Security in LoRaWAN Applications*, `https://smartmakers.io/en/security-in-lorawan-applications/`. Fetched on 21 August 2019.

[17] LoRa Alliance, *LoRaWAN^{TM}what is it? A technical overview of LoRa® and LoRaWAN^{TM}*, `https://www.tuv.com/media/corporate/products_1/electronic_components_and_lasers/TUeV_Rheinland_Overview_LoRa_and_LoRaWANtmp.pdf`. Fetched on 1 August 2019.

[18] A. Molich, *Wireless Communications*, 2nd ed.; John Wiley & Sons Ltd, The Atrium, Southern Gate, Chichester, West Sussex, PO19 8SQ, United Kingdom, 2011

[19] K. Yu, *3-D Localization Error Analysis in Wireless Networks*. IEEE Trans. Wirel. Commun.2007,6, 3473–3481.

[20] M. Khan, N. Salman, A. Kemp, L. Mihaylova, *Localisation of Sensor Nodes with Hybrid Measurements in Wireless Sensor Networks*, (2016) Sensors. 16. 1143. 10.3390/s16071143.

[21] S.M. Kay, *Fundamentals of Statistical Signal Processing: Estimation Theory*, 1st ed.; Prentice Hall: Upper SaddleRiver, NJ, USA, 1993.

[22] W. Liu, M. Kulin, T. Kazaz, A. Shahid, I. Moerman, E. De Poorter, *Wireless Technology Recognition Based on RSSI Distribution at Sub-Nyquist Sampling Rate for Constrained Devices*. Sensors 2017, 17, 208

[23] E. Mackensen, M. Lai and T. M. Wendt, "Bluetooth Low Energy (BLE) based wireless sensors," SENSORS, 2012 IEEE, Taipei, 2012, pp. 1-4. doi: 10.1109/ICSENS.2012.6411303

[24] Microchip Developer. Bluetooth® Low Energy Channels, https://microchipdeveloper.com/wireless:ble-link-layer-overview

[25] Bluetooth Special Interest Group, *Bluetooth Core Specification Version 5.1*, 2019. https://www.bluetooth.com/specifications/bluetooth-core-specification

[26] Microchip Dveloper. *Bluetoothh® Low Energy Discovery Process*, https://microchipdeveloper.com/wireless:ble-link-layer-discovery. Fetched on 1 August 2019.

[27] Panorama Antennas, http://www.panorama-antennas.com/site/index.php?route=product/product&product_id=94. Fetched on 15 August 2019.

[28] Shenzhen Chafon Technology, http://www.chafon.com/productdetails.aspx?pid=530. Fetched on 20 August 2019.

[29] M. Westenberg, *Single-Channel Gateway*, http://things4u.github.io/UserGuide/One%20Channel%20Gateway/Introduction%205.html. Fetched on 1 June 2019.

[30] Texim Europe, *Field Test Device LoRaWAN Europe* https://www.texim-europe.com/getfile.ashx?id=118476. Fetched on 1 June 2019.

Printed by Tryckeriet i E-huset, Lund 2019

LUND
UNIVERSITY

Series of Master's theses
Department of Electrical and Information Technology
LU/LTH-EIT 2019-720
http://www.eit.lth.se